AD-A168 971 THEORETICAL STUDY ON THE CORRELATION BETWEEN WIDEBAND ELECTROMAGNETIC SPE..(U) NORTH CAROLINA STATE UNIV AT RALEIGH DEPT OF MARINE EARTH AND.. I J WON APR 86 1/1

UNCLASSIFIED ARO-20065.2-GS DAAG29-83-K-0152 F/G 8/7 NL

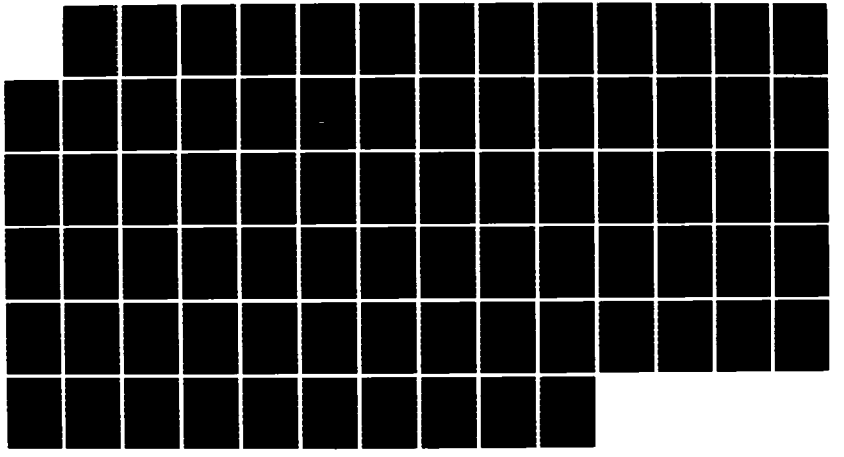

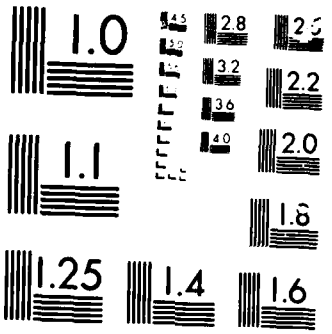

UNCLASSIFIED
SECURITY CLASSIFICATION OF THIS PAGE (When Data Entered)

REPORT DOCUMENTATION PAGE

READ INSTRUCTIONS BEFORE COMPLETING FORM

1. REPORT NUMBER: ARO 20065.2-GS	2. GOVT ACCESSION NO.: N/A
3. RECIPIENT'S CATALOG NUMBER: N/A	
4. TITLE (and Subtitle): Theoretical Study on the Correlation Between Wide-band Electromagnetic Spectra and Geological Structures	5. TYPE OF REPORT & PERIOD COVERED: 1 Sep 83 - 28 Feb 86 Final Report
	6. PERFORMING ORG. REPORT NUMBER
7. AUTHOR(s): I. J. Won	8. CONTRACT OR GRANT NUMBER(s): DAAG29-83-K-0152
9. PERFORMING ORGANIZATION NAME AND ADDRESS: North Carolina State University, Raleigh, NC 27695-8208	10. PROGRAM ELEMENT, PROJECT, TASK AREA & WORK UNIT NUMBERS
11. CONTROLLING OFFICE NAME AND ADDRESS: U. S. Army Research Office, Post Office Box 12211, Research Triangle Park, NC 27709	12. REPORT DATE: April 1986
	13. NUMBER OF PAGES: 52
14. MONITORING AGENCY NAME & ADDRESS (if different from Controlling Office)	15. SECURITY CLASS. (of this report): Unclassified
	15a. DECLASSIFICATION/DOWNGRADING SCHEDULE

16. DISTRIBUTION STATEMENT (of this Report)

Approved for public release; distribution unlimited.

17. DISTRIBUTION STATEMENT (of the abstract entered in Block 20, if different from Report)

NA

18. SUPPLEMENTARY NOTES

The view, opinions, and/or findings contained in this report are those of the author(s) and should not be construed as an official Department of the Army position, policy, or decision, unless so designated by other documentation.

19. KEY WORDS (Continue on reverse side if necessary and identify by block number)

Wide Band Electromagnetic Spectra
Electromagnetic Spectra
Geological Structures
Maxwell's Equations

20. ABSTRACT (Continue on reverse side if necessary and identify by block number)

A theoretical study has been performed to establish a mathematical means to compute the electromagnetic response of an earth having continuous and arbitrary conductivity variations, and to formulate a transfer function that can convert a wideband frequency-domain response to a continuous conductivity-depth function.

The study was based upon past experiences in both theoretical and experimental aspects of frequency-domain electromagnetic method. A new formal integral

DD FORM 1473 JAN 73 EDITION OF 1 NOV 65 IS OBSOLETE

UNCLASSIFIED

20. ABSTRACT CONTINUED

representation was formulated for Maxwell's equations for a medium having an arbitrary conductivity function. It was shown that the representation is suitable for forward problems and, through a proper integral transform, the inverse may possible exist. An attempt is being made to derive a transfer function that can convert an electromagnetic spectral response to a conductivity-depth profile.

Final Report

to

Army Research Office
Geoscience Division
Research Triangle Park, NC 27709

on

Theoretical Study on the Correlation Between Wideband Electromagnetic Spectra and Geological Structures

(ARO Contract Number: DAAG 29-83-K-0152)

by

I.J. Won

Associate Professor of Geophysics
Department of Marine, Earth, and Atmospheric Sciences
North Carolina State University
Raleigh, NC 27695-8208

April 1986

Table of Contents

1. Summary

We have performed under the subject contact a theoretical study i) to establish a mathematical means to compute the electromagnetic response of an earth having continuous and arbitrary conductivity variations, and ii) to formulate a transfer function that can convert a wideband frequency-domain response to a continuous conductivity-depth function.

The study is based upon our past experiences in both theoretical and experimental aspects of frequency-domain electromagnetic method. We present a new formal integral representation for Maxwell's equations for a medium having an arbitrary conductivity function. It is shown that the representation is suitable for forward problems and, through a proper integral transform, the inverse may possibly exist. An attempt is being made to derive a transfer function that can convert an electromagnetic spectral response to a conductivity-depth profile.

2. Introduction and Background

The frequency-domain electromagnetic (EM) method employing a single frequency or several frequencies up to the RF band has long been in use in the geophysical industry for investigating shallow geological structures in terms of anomalous electrical conductivity. The method, often referred to as the induction EM method, involves the propagation of low-frequency EM waves over the earth.

Ideally, an exploration method not only locates a sought target but also is able to describe it as a function of depth. One obvious approach which can provide both penetration and vertical resolution is a method employing a wide-band, multifrequency, or sweep-frequency source.

The groundwork for the EM method as an exploration tool for conductive mineral deposits has been well established as documented by Wait (1962), Keller and Frischknect (1966), Ward (1967), Patra and Mallick (1980), Kaufman and Keller (1983) and others. Although the method is based on the well-founded classical EM theory, the applications of the theory to realistic geological conditions have been limited to only simple cases.

During the past years, the principal investigator has been involved in studying the wideband induction EM response through both theory and experimentation. Using an integral equation representation for solving Maxwell's equation having inhomogeneous boundary conditions (Won and Kuo, 1975a and 1975b), we computed two-dimensional spectral profiles of a circular cylinder buried in a conductive half-space under a line source excitation. The secondary EM responses (without the primary field) are computed for a frequency range from 10 Hz to 40 KHz along the surface. Ensembles of such spectral profiles in a distance-frequency space are shown in Figure 1 for three depths of the circular cylinder (Won, 1980).

In order to test the theoretical results, we experimented with a scaled laboratory sweep-frequency EM system. The conductive earth was simulated with saline water while the target was made of graphite. Figure 2 shows experimentally obtained spectral responses for a vertical graphite slab submerged at three different depths (Won, 1980). Admittedly, the two models are dissimilar: a two-dimensional model of a circular cylinder with a line source cannot be compared rigorously with a vertical dike in the presence of a dipole source.

The spectral characteristics for both cases have been qualitatively known and are physically understandable. Rather, the main advantage of such wide-band spectral data is the method of cross-sectionally displaying the entire data to provide some intuitive interpretations: An anomaly caused by a large and deep structure will have a broad feature in space and will appear toward the lower end of the spectrum, while an anomaly caused by a small and shallow structure will have a narrow feature in space and will appear toward the higher end of the spectrum.

Encouraged by the results from the theoretical study and laboratory equipment, we developed and field-tested a first prototype sweep-frequency EM system mounted on a truck (Won, 1982 and 1983). A transmitter and receiver pair were used in a horizontal coplanar configuration employing logarithmically sweeping harmonic waves from 500 Hz to 80 kHz. The sweep duration was about 2 seconds at a maximum power of about 2 kW. Secondary field amplitude and phase spectra were measured, digitized, and stacked several times to enhance the signal-to-noise ratio. Data were collected while the truck was in transit (at about 5-10 MPH). The entire operation was automated by an on-board computer.

Figure 3 shows one of the spectral profiles obtained over a metamorphic terrain overlain by sediments of variable thicknesses with sporadic outcrops of graphite schist. The known cultural objects as well as available surface geological data are shown on an approximate geological section. The anomalies due to cultural objects such as bridges and culverts are easily recognizeable because their high-frequency anomalies are big enough to wipe out the entire spectral section. In contrast, geological anomalies are laterally and vertically extended showing a spatially distributed anomaly pattern. This particular profile was made at about 6 MPH by stacking five sweeps per station, each sweep lasting 2 seconds and having 70 discrete logarithmic frequency steps.

A spectral profile displayed in a frequency-distance space is somewhat analogous to a reflection seismic profile displayed in a time-distance space. Although the seismic diffraction theory is far from complete and more complicated than the EM diffraction theory, seismic reflection data are often self-evident in terms of the relative geometry of the reflecting boundaries. It is not to say that the conversion of a frequency-distance space EM data into a conductivity-depth section would be as definite as the conversion of a seismic time-distance section into a depth-distance section; the spectral EM theory must be developed much further to reach that stage.

In an analogy of a seismic (time-distance) section which, given the knowledge of the velocity distribution everywhere, can be converted to a depth-section, we may surmise that an EM spectral (frequency-distance) section, given the knowledge of the conductivity distribution everywhere, may be converted to a similar depth section. This report focuses on finding the theoretical linkage between the conductivity distribution and the geological cross-section through the understanding of wideband EM induction responses of the earth.

We have also applied successfully an airborne frequency-domain EM method to shallow ocean bathymetry (Won and Smit, 1985a) as well as measuring conductivities of water and bottom sediments (Won and Smits, 1985b). Figure 4 shows an exemplary bathymetric profile (solid line) compared to ground truth data (solid circles) obtained in Cape Cod Bay. We used two frequencies at 385 Hz and 7200 Hz both in horizontal coplanar configurations at a height of about 50 m above the ocean. The sensor was towed by a helicopter at a speed of about 90 knots. By analyzing the dual frequency data using a new inversion algorithm, we were able to determine simultaneously, water depth, water conductivity, and sediment conductivity. The method has a potential application to determining the ice-thickness profile in the polar region (Won and Smits, 1950). A separate comprehensive report on this subject is appended to this Final Report.

3. Theoretical Approach

One of the major shortcomings in the existing theories is that the earth model employed for their forward calculation is a layered earth with a finite number of layers, each having a distinct electrical conductivity. These can rarely be more than three to five layers in order to avoid numerical instability during inversion. Such a layering may be geologically unrealistic in most cases (since there is not a sufficient number of layers to account for gradual changes) and is believed to be the main source of instability in inverting real data. Therefore, the following equations are designed for the forward calculation of a laterally homogeneous earth with a continuous conductivity variation in depth.

The fundamental equations for the magnetic field generated by a vertical oscillating dipole located at the surface of a horizontally stratified earth have been given by Wait (1955), Kozulin (1963), and Frischknecht (1967). The following is the expression for the EM vector potential F generated in a point at or above the surface of the earth under conditions considered by Kozulin:

$$F_z = \frac{M}{4\pi}\left\{\frac{1}{\sqrt{r^2+(h-z)^2}} + \int_0^\infty R(\lambda, d_i, \sigma_i, \omega)\, J_0(\lambda r)\, d\lambda\right\} . \qquad (1)$$

The components of the vector potential in the horizontal plane are zero, and the radiation term in the Maxwell equation has been neglected.

The transmitting dipole is considered to be located at (0,-h) of the cylindrical coordinate system with the z-axis directed vertically downward. The point at which the vector potential is computed is located at (r,-z). The mathematical notations are as follows:

d_i thicknesses of the i-th subsurface layer,

σ_i conductivities of the i-th subsurface layer,

h transmitter height (negative upward)

z receiver height (negative upward)

λ variable of integration,

M dipole moment of the transmitter,

ω angular frequency of the transmitted signal,

μ magnetic permeability for free space, and

J_0, zeroth order Bessel function.

The kernel function $R(\lambda)$ can be computed from the subsurface layer parameters and the frequency using a recurrence relation. Setting $R(\lambda) = R_{0,n}(\lambda)$ in which the first suffix represents consideration of the field in space above the ground surface, and the second suffix n is the number of subsurface layers, the recurrence relation is given by [using the notation of Koefoed et al. (1972)]:

$$R_{(i-1),n}(\lambda) = \frac{V_{(i-1),i} + R_{i,n}(\lambda)e^{-2d_iV_i}}{1 + V_{(i-1),i}R_{i,n}(\lambda)e^{-2d_iV_i}} e^{-\lambda(h-z)} \qquad (2)$$

and

$$R_{n,n}(\lambda) = 0$$

where

$$V_i = (\lambda^2 + k_i^2)^{1/2},$$

$$k_i^2 = i\omega\mu\sigma(z), \text{ and}$$

$$V_{i,k} = (V_i - V_k)/(V_i + V_k).$$

The expressions for the components of the magnetic field strength can be obtained from (1). The relation between the magnetic field strength and the vector potential can be written as

$$\vec{H} = \nabla \nabla\cdot\vec{F} - k^2\vec{F} \qquad (3)$$

and consideration of the field in the space above the ground surface implies that $k^2 = k_0^2 = i\omega\mu_0\sigma_0 = 0$, reducing (3) to

$$\vec{H} = \nabla\ \nabla\cdot\vec{F}. \tag{4}$$

Recalling that the components of F in the horizontal plane are zero, we may rewrite (4) as

$$\vec{H} = \nabla\left(\frac{\partial}{\partial z} F_z\right)$$

or

$$H_z = \frac{\partial^2}{\partial z^2} F_z, \text{ and } H_r = \frac{\partial^2}{\partial z \partial r} F_z \tag{5}$$

Applying the differentiations to (1) and then setting z = 0, we have, for the components of the magnetic field strength at a point at the surface of the earth, the expressions

$$H_z = -\frac{M}{4\pi r^3} + \frac{M}{4\pi} \int_0^\infty \lambda^2 R(\lambda, d_i, \sigma_i, \omega) J_0(\lambda r) d\lambda, \tag{6}$$

$$H_r = \frac{M}{4\pi} \int_0^\infty \lambda^2 R(\lambda, d_i, \sigma_i, \omega) J_1(\lambda r) d\lambda \tag{7}$$

where J_0 and J_1 are Bessel functions of the first kind. The first term in (6) represents the primary field in the absence of the earth while the second term denotes the secondary field. Only the secondary field exists for the radial component.

The recurrence formula (2) is widely used for computing the EM responses of a multilayered earth. The infinite integrals shown by (6) and (7) are often computed numerically using a Hankel transform algorithm or digital filter method (Koefoed et al, 1973; Anderson, 1979 and 1982; Chave, 1983). The main shortcoming is that these methods are strictly limited to discretely layered earth models.

4. Mathematical Formulation for an Earth having a Continuous Conductivity Variation

We now consider a transformation of the kernel function $R(\lambda)$ in an integral form which can handle a continuously-varying conductivity function $\sigma(z)$. Our present goal is to express the magnetic field as an integral equation containing a continuous function $\sigma(z)$. Such expressions are highly desirable for interpreting our swept-frequency data.

In order to change $R(\lambda)$ to a differential form, we first let the thickness of each layer d_i be Δz, a vanishingly small distance. Under this condition, the terms appearing in (2) can be shown as follows:

$$V_{(i-1),i} = \frac{V_{i-1} - V_i}{V_{i-1} + V_i} = -\left\{\frac{1}{2\sqrt{\lambda^2+k^2(z)}} \frac{d}{dz} \sqrt{\lambda^2+k^2(z)}\right\} \cdot \Delta z$$

$$= \frac{-1}{4\{\lambda^2+k^2(z)\}} \frac{\Delta k^2(z)}{\Delta z} \cdot \Delta z \qquad (8)$$

and

$$d_i V_i = \Delta z \sqrt{\lambda^2+k^2(z)} \quad . \qquad (9)$$

Here we assume that $k(z)$ is continuous and its first derivative exists. This is found to be the main condition for departing from the traditional layered earth model. It can be seen that while the two numerator terms in (2) are in the first order of Δz, their product appearing in the denominator is in the second order of Δz. For the limiting case, therefore, we may write equation (2) as

$$R_{(i-1),n}(\lambda) = V_{(i-1),i} + R_{i,n}(\lambda) e^{-2d_i V_i} \quad . \qquad (10)$$

Expanding this and using its own recurrence relationship, we find

$$R(\lambda) = R_{0,n}(\lambda) = V_{0,1} + V_{1,2} e^{-2d_1 V_1} + V_{2,3} e^{-2(d_1 V_1 + d_2 V_2)}$$

$$+ V_{3,4} e^{-2(d_1 V_1 + d_2 V_2 + d_3 V_3)} + \cdots\cdots + V_{n,n+1} e^{-2(d_1 V_1 + \cdots + d_n V_n)} + \cdots$$

$$= \sum_{0}^{\infty} V_{n,n+1} \exp\left(-2\sum_{1}^{n} d_i V_i\right) . \qquad (11)$$

As we let $\Delta z \to 0$, we may express (11) in an integral form:

$$R(\lambda) = -\frac{1}{2}\int_{0}^{\infty} \frac{1}{V}\frac{dV}{dz} \exp\left\{-2\int_{0}^{z} V(\xi)d\xi\right\}dz \qquad (12)$$

where $V(z) = \sqrt{\lambda^2+k^2(z)}$. The exponential term denotes physically a two-way attenuation in depth while the remaining terms can be interpreted as an inductive coupling within the earth medium. Since the exponential term is dominant, we would generally expect a stable and convergent integration.

The secondary vertical magnetic field $H_z^s(\omega,r)$, the second term in (6), can now be written as

$$H_z^s(\omega,r) = -\frac{M}{8\pi}\int_{0}^{\infty}\lambda^2 J_0(\lambda r)\int_{0}^{\infty}\frac{1}{V(z)}\frac{dV(z)}{dz}\exp\left\{-2\int_{0}^{z}V(\xi)d\xi\right\}dz d\lambda . \qquad (13)$$

Changing the order of integration between z and λ, and using the relationship

$$\frac{1}{V}\frac{dV}{dz} = \frac{1}{2\{\lambda^2+k^2(z)\}}\frac{dk^2(z)}{dz} \qquad (14)$$

we may rewrite (13) as

$$H_z^s(\omega,r) = -\frac{M}{8\pi}\int_{0}^{\infty}\frac{dk^2(z)}{dz}\int_{0}^{\infty}\frac{\lambda^2 J_0(\lambda r)}{\lambda^2+k^2(z)}\exp\left\{-2\int_{0}^{z}\sqrt{\lambda^2+k^2(\xi)}\,d\xi\right\}d\lambda dz. \qquad (15)$$

The λ-integral can be evaluated by the residue theorem. We first note that the integral is symmetrical in λ; thus, its range can be expanded to negative infinity. We find two simple poles in the second and fourth quadrants at $\lambda = \pm k$. Also, the integration along an infinite semi-circle in the upper half of the complex plane can be shown to be zero. The integral, therefore, can be represented by the residue at the second quadrant and, thus,

$$H_z^s(\omega,r) = \frac{iM}{8}\int_0^\infty k^2(z)J_0(ikr)\frac{dk^2(z)}{dz}\exp\{-2\int_0^z \sqrt{k^2(z)-k^2(\xi)}\,d\xi\}\,dz. \quad (16)$$

Equation (16) represents a significant improvement over (6) in the sense that it is the first expression by which we can compute the EM response over an earth model having a continuous conductivity function. Once $\sigma(z)$ and its derivative are specified, the integral can be evaluated either analytically or numerically depending upon the complexity of the conductivity function. Its convergence is facilitated owing to the exponential attenuation term.

Our ultimate goal is to invert equation (16) so that $\sigma(z)$ can be determined at each data point for a given wideband spectrum $H(\omega,r)$ at $r=a$, a constant transmitter-receiver separation. We plan to continue our investigation on possibilities of analytically inverting (16) through integral transform techniques. Otherwise, we may be forced to solve (16) numerically. A popular technique for numerically solving integral equations is the moment method as described by Harrington (1968). The method, in essence, is an approximate linearization process which assumes a certain functional for the unknown in a whole range or in each subsectional range. This process reduces the integral equation into a set of matrix equations which is inverted numerically.

Equations (6), (7) and (16) can be also viewed as convolution integrals: it has been well known that the Hankel transform integrals can be transformed to a linear convolution-type integral through proper substitutions of variables (Ghosh, 1971; Koefoed et al., 1972; Anderson, 1979 and 1982). If the continuous convolution is discretized, the resultant discrete linear convolution becomes simply a linear digital filter of a finite length.

We may formally treat Equation (16) is a similar way: the filter acts on

a kernel function representing the conductivity distribution $\sigma(z)$ and its vertical derivative. The filtered output corresponds to the spectral response of the magnetic field $H(\omega)$. Therefore, if we can find a inverse filter (or a transfer function), we will be able to convert the spectral response $H(\omega)$ to the conductivity function $\sigma(z)$. Finding an inverse of a given linear digital filter is a highly advanced subject of deconvolution, and a variety of approaches are available particularly for seismic signal processing (e.g., Robinson, 1983).

5. Conclusion

Despite the fact that the layered earth model has been studied by many researchers, the model has not been used comprehensively in terms of its spectral responses. Other than for a low frequency range mostly using natural sources such as those in MT survey, the EM method measuring continuous spectral response rarely has been considered as a stratigraphic mapping tool. While the EM method is used mainly for locating isolated conductive orebodies, there is a strong theoretical possibility that the method can be expaned for wide use utilizing the spectral profiles displayed in a frequency-distance space.

The progress of the subject research is still elementary considering the complex geological nature. Yet, the task is believed to be a timely and essential step in enhancing the capability and further development of a wideband (ground or airborne) electromagnetic exploration method applicable to geological, geophysical, and geotechnical mapping of complex three-dimensional earth structures.

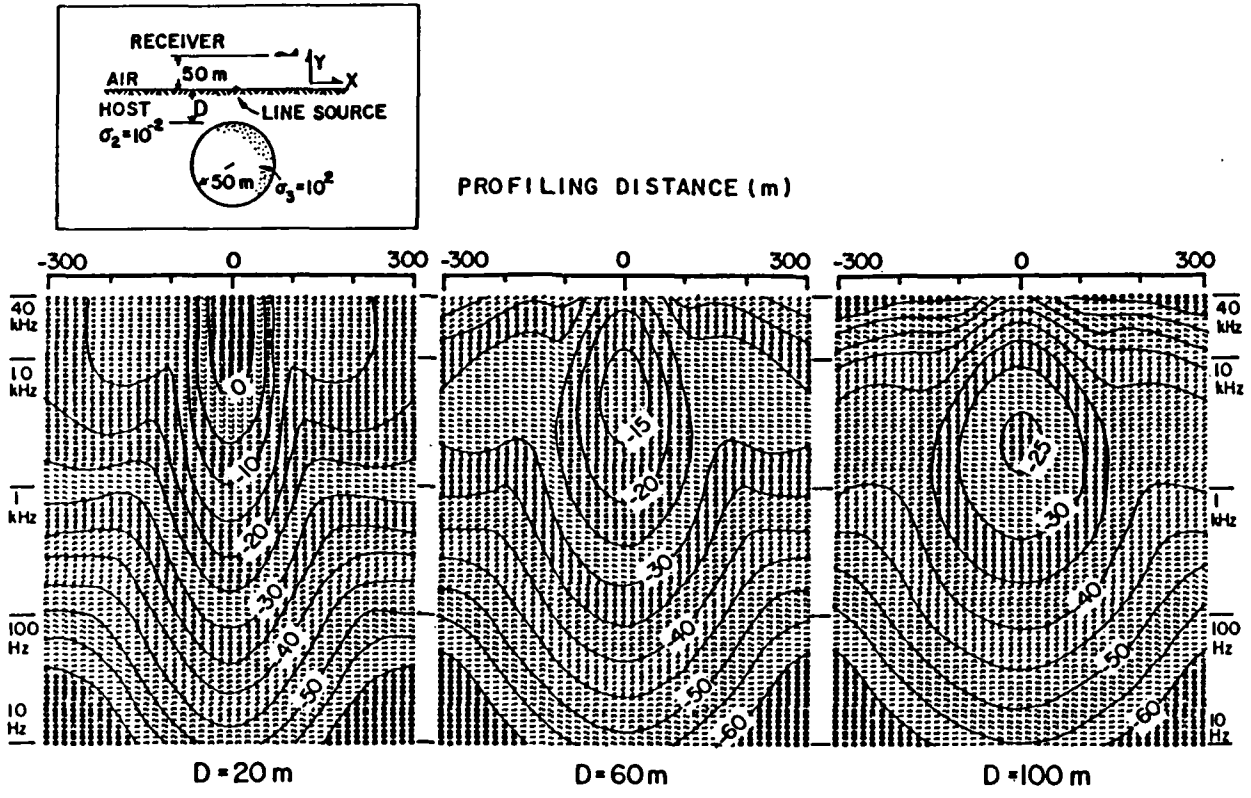

Figure 1. Theoretically computed amplitude spectral profiles of horizontal magnetic field for the situation shown in the inset for various depths: 20, 60 and 100 m. The horizontal axis denotes the profiling distance of the receiver extending 300 m on either side fo the circular cylinder located at the center of the profile. Any single-frequency profile may be obtained by selecting a specific frequency on the vertical scale. The contour interval is 5 dB with an arbitrary reference.

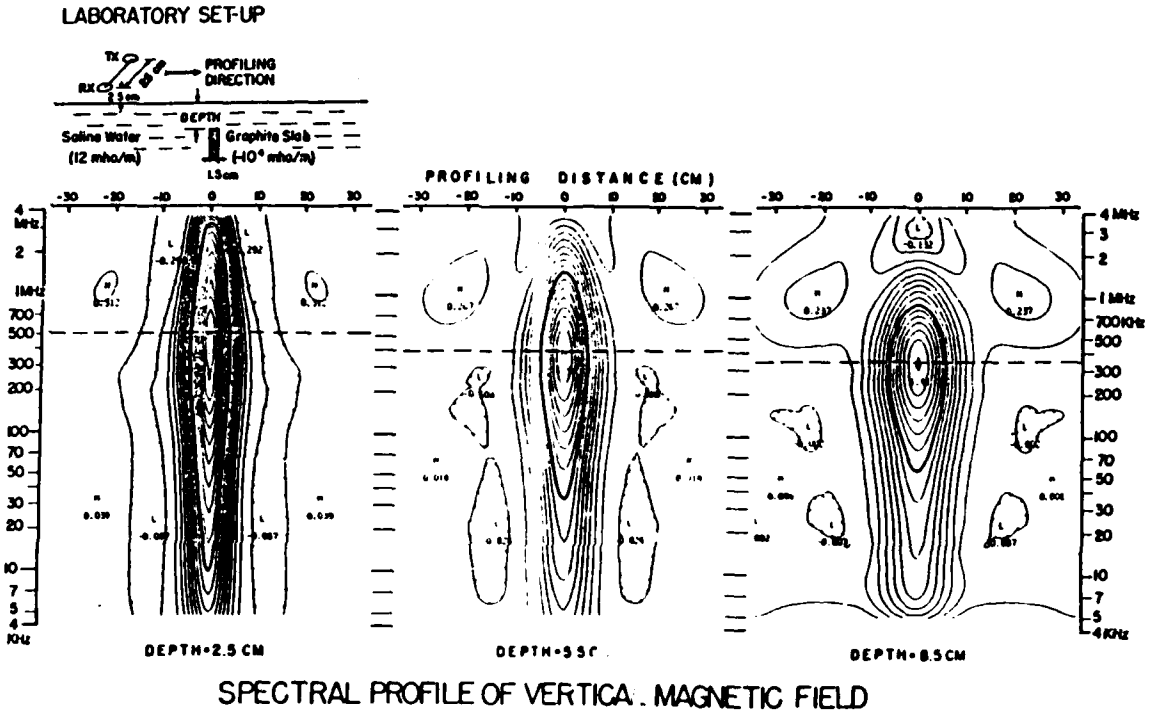

Figure 2. Experimentally obtained amplitude spectra of magnetic field of a buried dike in a conductive half-space employing a horizontal coils system in a scaled model set-up.

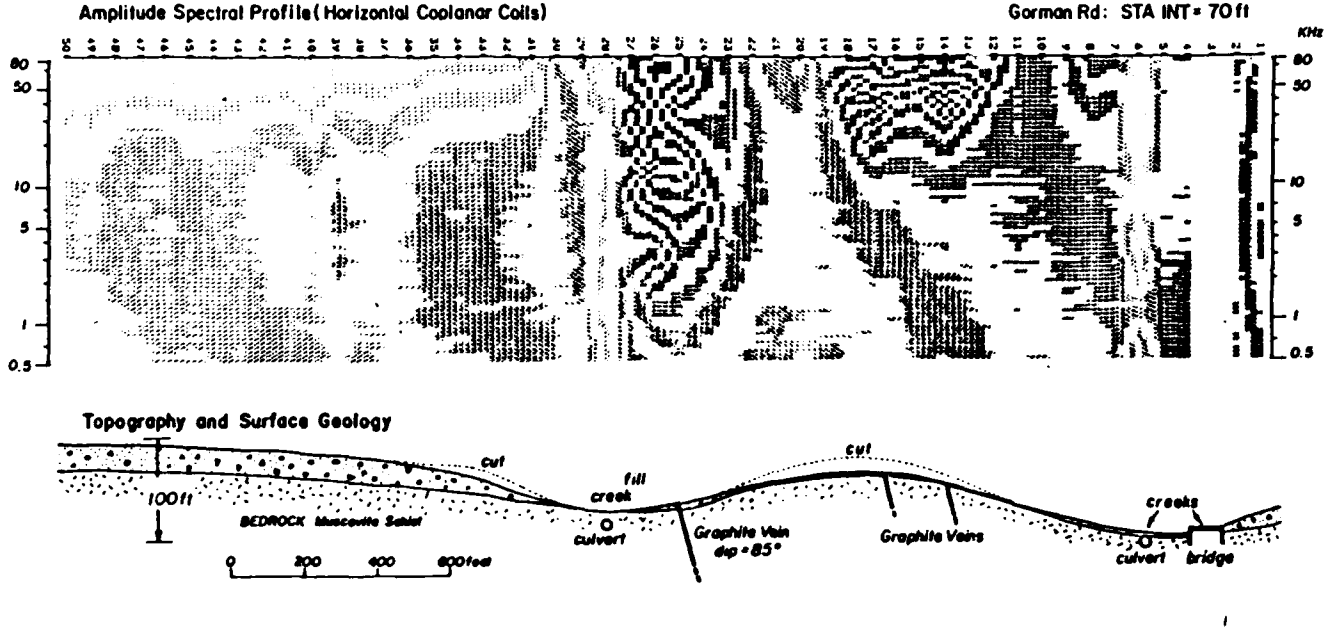

Figure 3. Amplitude spectral profile from a portion of Gorman Road, southern Raleigh, NC, along with available geological data and cultural objects.

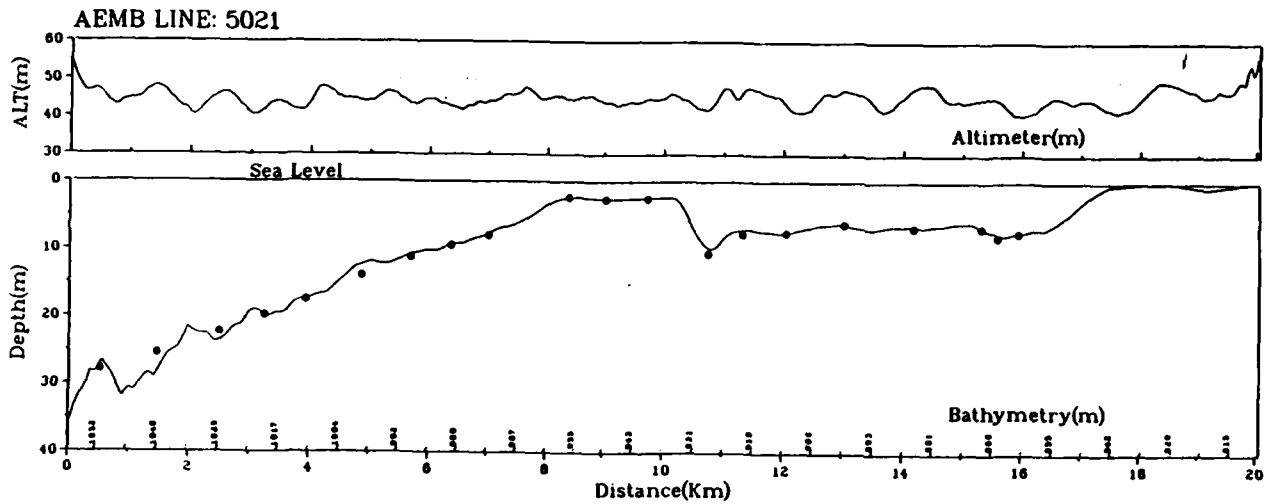

Figure 4. AEM bathymetric profile for Line 5021 along with radar altimeter profile. Solid line represents AEM bathymetry; while solid circles represent depths obtained from a shipborne acoustic profiler. Small numerals at bottom are the flight fiducials.

References

Anderson, W.L. (1979). Numerical integration of related Hankel transforms of order 0 and 1 by adaptive digital filtering, Geophysics, v. 44, pp. 1287-1305.

Anderson, W.L. (1982). Fast Hankel transforms using related and lagged convolutions, ACM Trans. on Math. Software, V. 8, pp. 344-368.

Chave, A.D. (1983). Numerical integration of related Hankel transforms by quadrature and continued fraction expansion, Geophysics, v. 48, pp. 1671-1686.

Frischknecht, F.C. (1967). Field about an oscillating magnetic dipole over a two-layer earth and application to ground and airborne electromagnetic surveys, Quarterly of the Colorado School of Mines, v. 62, n. 1, pp. 1-370, Golden.

Ghosh, P.P., (1971). The application of linear filter theory to the direct interpretation of geoelectrical resistivity sounding measurements, Geophys. Prop., v. 19, p. 192-217.

Harrington, R.F. (1968). Field computation by moment methods, Macmillan Co., New York, 229 pp.

Kaufman, A.A. and G.V. Keller, (1983). Frequency and Transient Soundings, Elsevier, Amsterdam, 685 pp.

Keller, G.V. and Frischknecht, F.C. (1966). Electrical Methods in Geophysical Prospecting: New York, Pergamon Press, 517 pp.

Koefoed, O., D.P. Ghosh, and G.J. Polman (1972). Computation of type curves for electromagnetic depth sounding with a horizontal transmitting coil by means of a digital linear filter. Geophysical Prospecting, v. 20, pp. 406-420.

Kozulin, Y.N. (1963). A reflection method for computing the electromagnetic field above horizontal lameller structure. Izvestiya, Academy of Sciences, USSR, Geophysics Series (English Edition), no. 3, pp. 267-273.

Patra, H.P., and Mallick, K. (1980). Time-Varying Geoelectric Soundings, Geosounding Principles 2, Methods in geochemistry and Geophysics, 14B, Elsevier Scientific Pub. Co., Amsterdam, 419 pp.

Robinson, E.A. (1983). Multichannel Time Series Analysis with Digital Computer Programs, Second Ed., Goose Pond Press, Houston, 454 pp.

Wait, J.R. (1955). Mutual electromagnetic coupling of loops over a homogeneous ground, Geophysics, v. 20, pp. 630-637.

Wait, J.R. (1962). Electromagnetic Waves in Stratified Media, Pergamon Press, New York, 372 pp.

Ward, J.R., (1962). Electromagnetic Waves in Stratified Media, Pergamon Press, New York, 372 pp.

Won, I.J. and J.T. Kuo (1975a). Representation theorems for multiregional electrodynamic diffration; Theory, Geophysics, v. 40, pp. 96-108.

Won, I.J. and J.T. Kuo (1975b). Representation theorem for multiregional electrodynamic diffraction; Applications, Geophysics, v. 40, pp. 109-119.

Won, I.J. (1980). A wideband electromagnetic exploration method---some theoretical and experimental results, Geophysics, v. 45, 928-940.

Won, I.J. (1982). Development of a prototype sweep-frequency electromagnetic exploration system, Extended Abstract, Society of Exploration Geophysicists Annual Meeting Program, pp. 397-399.

Won, I.J. (1983). A sweep-frequency electromagnetic exploration method, Chapter 2, in Development in Geophysical Exploration Methods -4, pp. 39-64, Ed. A.A. Fitch, Applied Science Publishers, Ltd., London.

Won, I.J. and K. Smits, (1985a). Airborne electromagnetic bathymetry, Naval Ocean Research and Development Activity (NORDA) Report 94, 18 pp.

Won, I.J. and K. Smiths, (1985b). Characterization of shallow ocean sediments using the airborne electromagnetic method, Naval Ocean Research and Development Activity (NORDA) Report 106, 19p. (also accepted for publication in IEEE Journal of Ocean Engineering).

Won, I.J. and K. Smits (1985c). Frequency-domain electromagnetic ice-sounding, in Proceeding of the Arctic Oceanography Conference, pp. 167-172, NSTL, Mississippi.

Appendix to

Final Report on
ARO Contract Number DAAG29-83-K-0152

April 1986

Application of the Frequency-domain Electromagnetic Method to Airborne Bathymetry

by

K. H. Son and I. J. Won

Department of Marine, Earth, and Atmospheric Sciences
North Carolina State University
Raleigh, North Carolina 27695-8208

ABSTRACT

Airborne Electromagnetic Bathymetry (AEMB) is a recently developed technique for determining the depth of shallow sea water, using an airborne electromagnetic method. The transmitting and receiving loops are encased in a rigid tube and towed behind an aircraft at an altitude of about 140 feet. The relatively simple geometry of the shallow sea water environment provides us some practical advantages in survey design and data interpretation, while the small skin depth associated with highly conductive sea water requires low frequency which makes the AEMB problem a major challenge.

Application of geophysical inverse theory (nonlinear and linear) combined with two-layer model simulating sea water and bottom sediment provides us valuable information toward survey design and data interpretation. Uncertainty in the sensor altitude is resolved through the inversion process using high frequency data for which the ocean may be considered as an infinite half-space. The effect of variation of the coil axis with respect to the sea surface can be resolved if the inclination is measured and incorporated into the inversion process. An optimum frequency range for a given bathymetric range may be determined in advance by analyzing the information density matrix. For a reliable bathymetric determination, at least one low frequency whose skin depth is close to water depth need be included. High

frequencies whose skin depths are less than 1/4 - 1/3 of the water depth do not contribute significantly to the bathymetric solution, however the high frequency data can be used to determine the conductivity of sea water and to correct for the error in the altimeter height of the aircraft.

Since the conductivity of the sediment is proportional to the porosity of sediments following Archie's Law, it is expected to be decaying with depth. A theoretical electromagnetic response over exponentially decaying conductivity material underlain by sea water has been derived and compared with that of layered earth.

INTRODUCTION

Recently, there has been an increasing interest in possible airborne determination of bathymetric depth over shallow water (lakes and coastal bays). Becker et al. (1984) have considered the Airborne Electromagnetic Bathymetry problem by time-domain electromagnetic (TDEM) method. In this paper, we will present a fundamental theory for the Airborne Bathymetry by electromagnetic frequency sounding method.

Unlike cases of buried conductive layers under resistive overburden, the airborne electromagnetic bathymetry (AEMB) is to determine the depth of highly conductive sea water over relatively resistive bottom sediments (Figure 1). It is understandably a difficult problem to determine the bottom geometry of the sea floor by electromagnetic induction method; because of the high conductivity of sea water, EM energy attenuates rapidly with depth and, thus, the effect of the bottom geometry on the returned signal is small. The resolution is dependent upon the accuracy of the measured data and their frequency content.

In the airborne survey, the transmitting and receiving loops are usually encased in a rigid tube or a truss support (generally called a 'bird') which is towed behind the aircraft on a guywire. Height is measured by a radar altimeter usually mounted on the aircraft. Horizontal levelling of the bird could be monitored by an inclinometer. Modern

instruments under ideal conditions can resolve the secondary EM response up to 1 ppm or better with respect to the primary field. A study in this paper shows that small errors in the positioning of the bird can cause as much effect as that of bottom geometry of sediments, indicating that correction of the data must be made before interpretation.

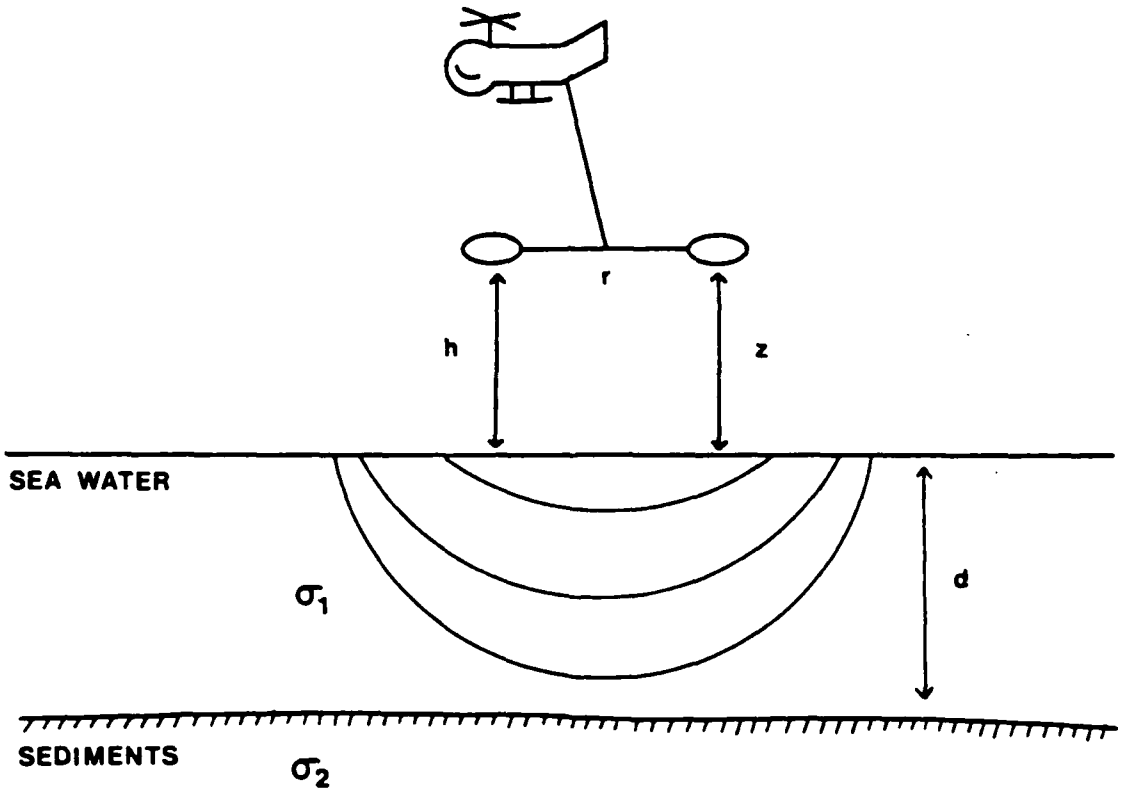

Figure 1 Geometry of Airborne Electromagnetic Bathymetry.

Because of the skin effect of EM wave, the deeper sea water becomes, the lower frequency we need to properly resolve the deep structure. Technically, it is more difficult to generate a lower frequency (below 100 Hz) than to generate a higher frequency; the large dipole moment demanded for low frequency requires an extra large coil and a high current source which, in turn, increases on-board logistics, weight, and power requirements. In addition, the spatial resolution also suffers as frequency is lowered. Therefore it is ideal that optimal range of frequency be determined for a given range of water depth. The result of this study shows that, to determine basement geometry with data measured at 10 m altitude and 10 m separation, we need at least a frequency whose skin depth is the same as the depth of investigation, and we do not need those frequencies whose skin depths are less than 1/3 - 1/4 of depth of investigation.

Once the data are corrected properly, the parameter most strongly influencing the data is the lateral variation of conductivity of sea water. The next most significant parameter is the thickness of the sea water layer. The conductivity of bottom sediments has the smallest effect. According to Grant and West (1965), sea water conductivity varies between 2.5 and 5.0 (mho/m), and normal basement conductivity is in the range of 0.0 to 0.4 (mho/m). The conductivity of basement water or transition-zone sediments varies between 0.0001 and 1.0 (mho/m). Since the target of

an AEMB survey may be considered to be shallow, increasingly deepening water (less than 100 m in depth) on the continental shelf, we will simplify the model as follows:

i) the stratification of conductivity within sea water will be neglected,

ii) since the slope of sediments is gentle, the boundary of water and sediments will be assumed to be horizontal for each set of data, and

iii) the conductivity variation of sediments with depth will be neglected until later section. However, to account for this oversimplification, upper and lower bounds will be sought for the solution.

These simplifications, lead us to deal with a two-layer model with three unknowns, viz, sea water conductivity (σ_1), water depth (d), and bottom sediment conductivity σ_2. The interpretation technique employing Marquardt's (1963, 1970) technique and generalized inverse theory (Wiggins, 1972; Jackson, 1972; Inman et al., 1973) can be used for this two-layer model. Applied to synthetic data, the technique produces an accurate determination of the sea water conductivity. The determination of two other unknowns, depth of sea water and conductivity of sediments, is dependent upon the frequency range used and errors involved in the data. 'Edge model' is defined as a maximum or minimum depth of water for a given condition; since sea water conductivity is determined accurately, the lower bound is found by expanding the water depth until the rms difference between the data and

the predicted response becomes a tolerable preset value, assuming an insulating ocean bottom. Similarly, the upper bound is found by assuming 0.4 mho/m as the maximum conductivity of bottom sediments.

We will first review the response function of vertical and horizontal dipoles over a layered earth. Next, the efforts will be concentrated on the method of correcting the errors which can be caused by mispositioning of dipoles in airborne measurements, and on the optimum frequency range design of airborne EM bathymetry by using the generalized inverse theory. An application to synthetic data will be illustrated. Finally, a theoretical electromagnetic response over exponentially decaying conductive material underlain by sea water will be presented.

RESPONSE OF A WATER LAYER OVER SEDIMENTS

In the very low frequencies (VLF) where the frequency range is below 100 kHz, the effect of the dielectric constant which governs the displacement current within the target materials is small (for water $\epsilon/\epsilon_0 = 80$). Magnetic susceptibilities of sea water, or sediments are essentially zero, the same as that of air. For most crystalline rocks, it is small unless they contain considerable amounts of magnetite. The main physical property governing the electromagnetic field is the electrical conductivity. Therefore, the response functions of layered earth model (Wait, 1951; Frischknect, 1967; Ward, 1967; Patra and Mallick, 1980; Kaufman and Keller, 1983) are valid for the bathymetry problem.

Since the transmitting and receving loops are encased in a rigid tube or a truss support in the AEMB measurement, the primary field is dependent upon radial distance only. Using similar notation as Frischnecht (1967), the magnetic fields due to a vertical magnetic dipole over a layered earth (Figure 1) become

$$H_z^p = -\frac{M}{4\pi r^3} \qquad (1)$$

$$H_z^s = \frac{M}{4\pi} t_0 \qquad (2)$$

$$H_r^s = \frac{M}{4\pi} t_1 \ , \qquad (3)$$

and those due to a horizontal magnetic dipole,

$$Hr^{p} = -\frac{M}{2\pi r'^{3}} \qquad (4)$$

$$Hz^{s} = -\frac{M}{4\pi} t_1 \qquad (5)$$

$$Hr^{s} = \frac{M}{4\pi} \left(t_0 - \frac{1}{r} t_2 \right) \qquad (6)$$

where Hz^{p} is the z component of a primary field due to a vertical magnetic dipole, Hr^{p} is the r component of a primary field due to a horizontal magnetic dipole, and Hz^{s} and Hr^{s} are the z component and r component of secondary magnetic field, respectively. M is the dipole moment, r' is the distance from the transmitting dipole, and r is the horizontal component of r'. The t_0, t_1, and t_2 in equations (2) (6) are defined as

$$t_0 = \int_0^\infty \lambda^2 R(\lambda) e^{-\lambda(h+z)} J_0(\lambda r) d\lambda \qquad (7)$$

$$t_1 = \int_0^\infty \lambda^2 R(\lambda) e^{-\lambda(h+z)} J_1(\lambda r) d\lambda \qquad (8)$$

$$t_2 = \int_0^\infty \lambda R(\lambda) e^{-\lambda(h+z)} J_1(\lambda r) d\lambda \qquad (9)$$

where λ is a variable of integration and $R(\lambda)$ is the kernel function related to the geological parameters. The h and z are the heights of transmitting and receiving loops, respectively. J_0 and J_1 are Bessel functions of order zero and one, respectively. For a two-layer model the kernel function is given by (Patra and Mallick, 1980)

$$R(\lambda) = \left(\frac{n_0 - n_1}{n_0 + n_1} + \frac{n_1 - n_2}{n_1 + n_2} e^{-2dn_1} \right) \Big/ \left(1 + \frac{n_0 - n_1}{n_0 + n_1} \frac{n_1 - n_2}{n_1 + n_2} e^{-2dn_1} \right) \qquad (10)$$

where $n_i = \sqrt{\lambda^2 + j\omega\mu\sigma_i}$ in which i represents each layer, $j = \sqrt{-1}$, w angular frequency, μ magnetic permeability and σ_i is the conductivity of each layer.

Dividing secondary fields by their primary fields, we obtain mutual impedance ratios;

$$Z_1 = - r'^3 t_0 \quad , \tag{11}$$

$$Z_2 = - r'^3 t_1 \quad , \tag{12}$$

$$Z_4 = 1/2 \cdot (Z_3 - Z_1) \quad , \tag{13}$$

where $$Z_3 = - (r'^3 / r) t_2 \quad . \tag{14}$$

Z_1 represents a mutual impedance ratio of vertical-vertical dipoles. Z_2 represents a mutual impedance ratio of perpendicular dipoles (when the source dipole is horizontal, Z_2 must be multiplied by two). Z_4 represents a mutual impedance ratio of horizontal-horizontal dipoles whose axes are in the same direction, whereas Z_3 represents that of horizontal-horizontal dipoles which are in the common plane. When the heights of transmitting and receiving loops are kept the same, the configurations are called horizontal coplanar, perpendicular, vertical coaxial and vertical coplanar systems, respectively (Figure 2).

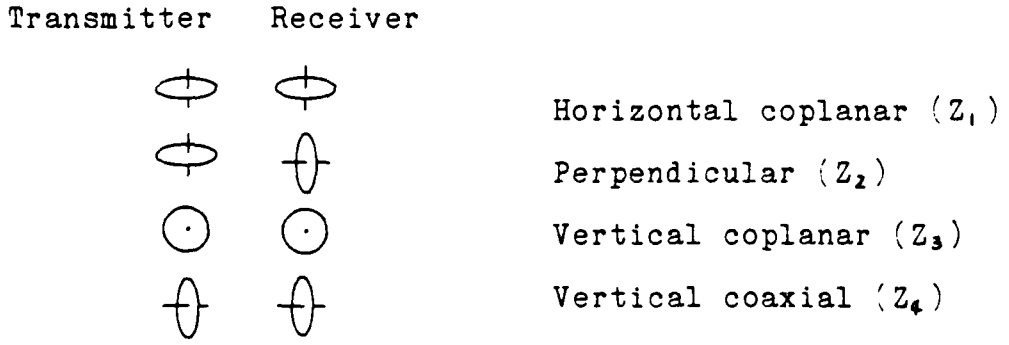

Figure 2 Four different configurations for vertical and horizontal magnetic dipoles.

Several Z_1 response curves are shown in Figures 3 through 5 for a two-layer model of which the first layer is a highly conductive layer simulating a sea-water layer underlain by a uniform half-space of resistive bottom sediments. The σ_1 and σ_2 represent the conductivity of water and sediment, respectively. The d represents thickness of the water body. In Figure 3, quadrature(imaginary), inphase(real) and amplitude of the Z_1 response, in ppm are illustrated for a two-layer model (top) of which σ_1 = 2 mho/m, σ_2 = 0.2 mho/m and d = 12 m. The response curves are computed at a 10 m height with a 10 m coil separation in a frequency range of 10 Hz and 100 kHz, and presented in log-log scale. Figure 4.a shows the effect of changing depth while keeping the conductivities and other parameters the same in the model. Figure 4.b shows the effect of changing σ_1 . Figure 4.c shows the effect of changing σ_2. Figure 5 illustrates the effect of changing r and h. Figures 4.a, 4.b, and 4.c show clearly that for the fixed r and h, the conductivity σ_1 of first layer has the most significant effect, followed by depth, and σ_2 in a descending order in significance. One interesting feature is that the skin depth of water at a frequency where the imaginary component becomes a maximum coincides roughly with the depth of water. In Figure 5, we also notice that inaccuracy in height and separation of the bird can cause significant effect for the geological interpretation.

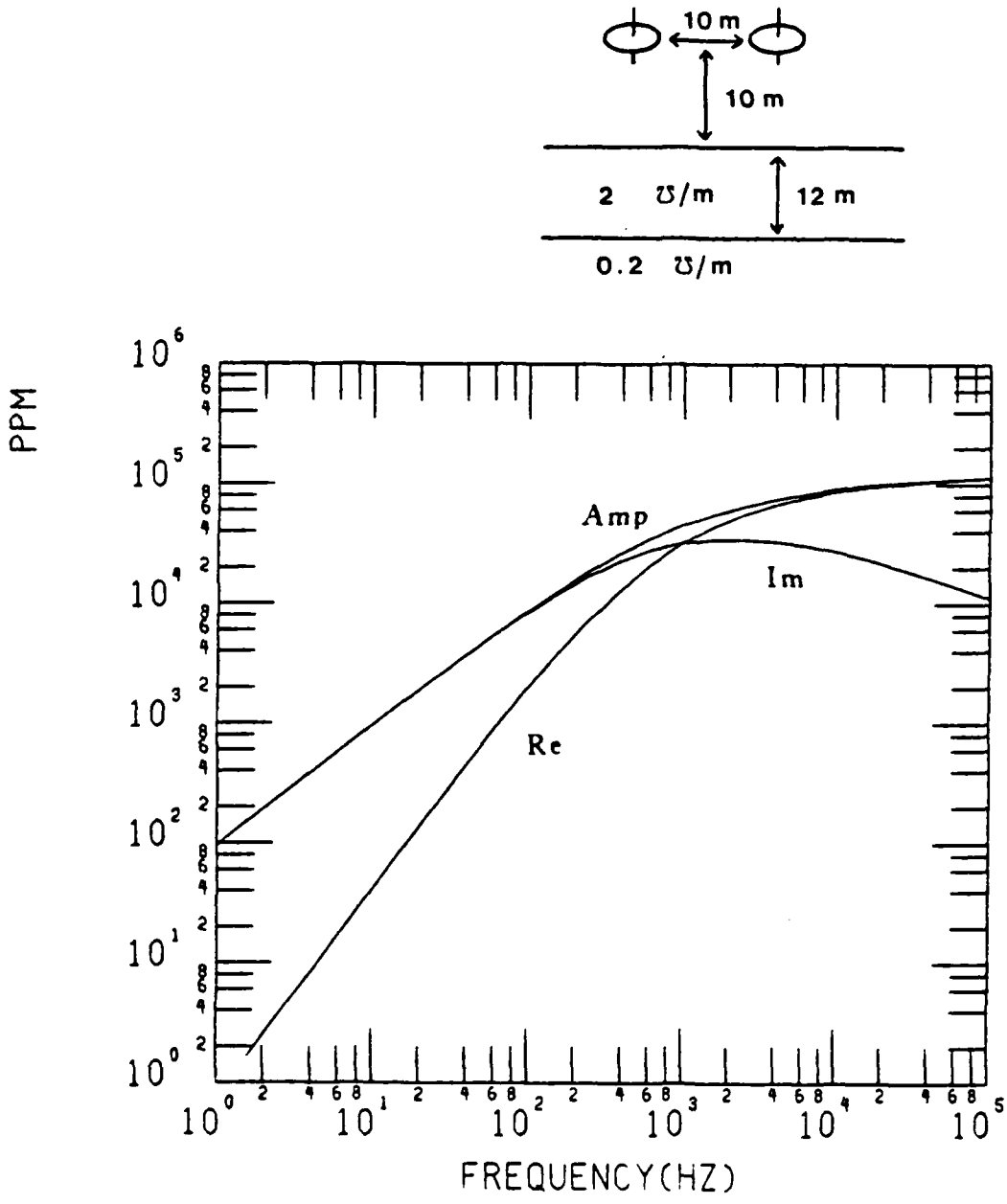

Figure 3 Mutual impedance ratio of a two-layer model (top), in ppm. Amp, Re and Im represent Amplitude, Real and Imaginary components of horizontal coplanar system, respectively.

Figure 4 Effects of parametric changes for the model shown on Figure 3 (σ_1 = 2 mho/m, σ_2 = 0.2 mho/m, d = 12 m r = h = 10 m), while keeping the other parameters the same
a. Effect of changing depth (5, 10, 20, 40, 80 m)
b. Effect of changing water conductivity (10, 5, 2, 1, 0.5 mho/m)
c. Effect of changing bottom conductivity (2, 1, 0.4, 0.1, 0.001 mho/m)

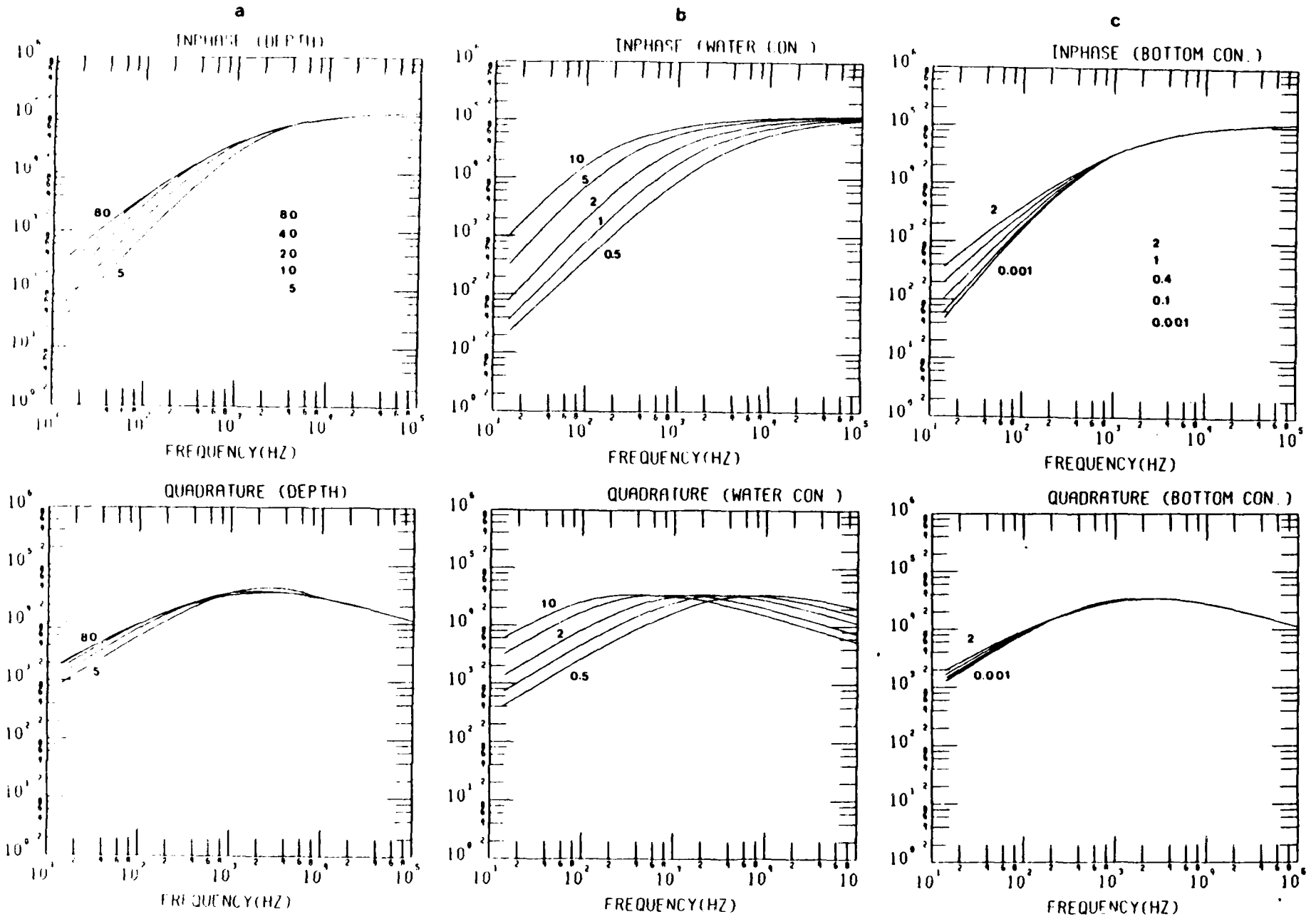
a
INPHASE (DEPTH)
80
5
80
40
20
10
5
FREQUENCY(HZ)
b
INPHASE (WATER CON.)
10
5
2
1
0.5
FREQUENCY(HZ)
c
INPHASE (BOTTOM CON.)
2
0.001
2
1
0.4
0.1
0.001
FREQUENCY(HZ)
QUADRATURE (DEPTH)
80
5
FREQUENCY(HZ)
QUADRATURE (WATER CON.)
10
2
0.5
FREQUENCY(HZ)
QUADRATURE (BOTTOM CON.)
2
0.001
FREQUENCY(HZ)

Figure

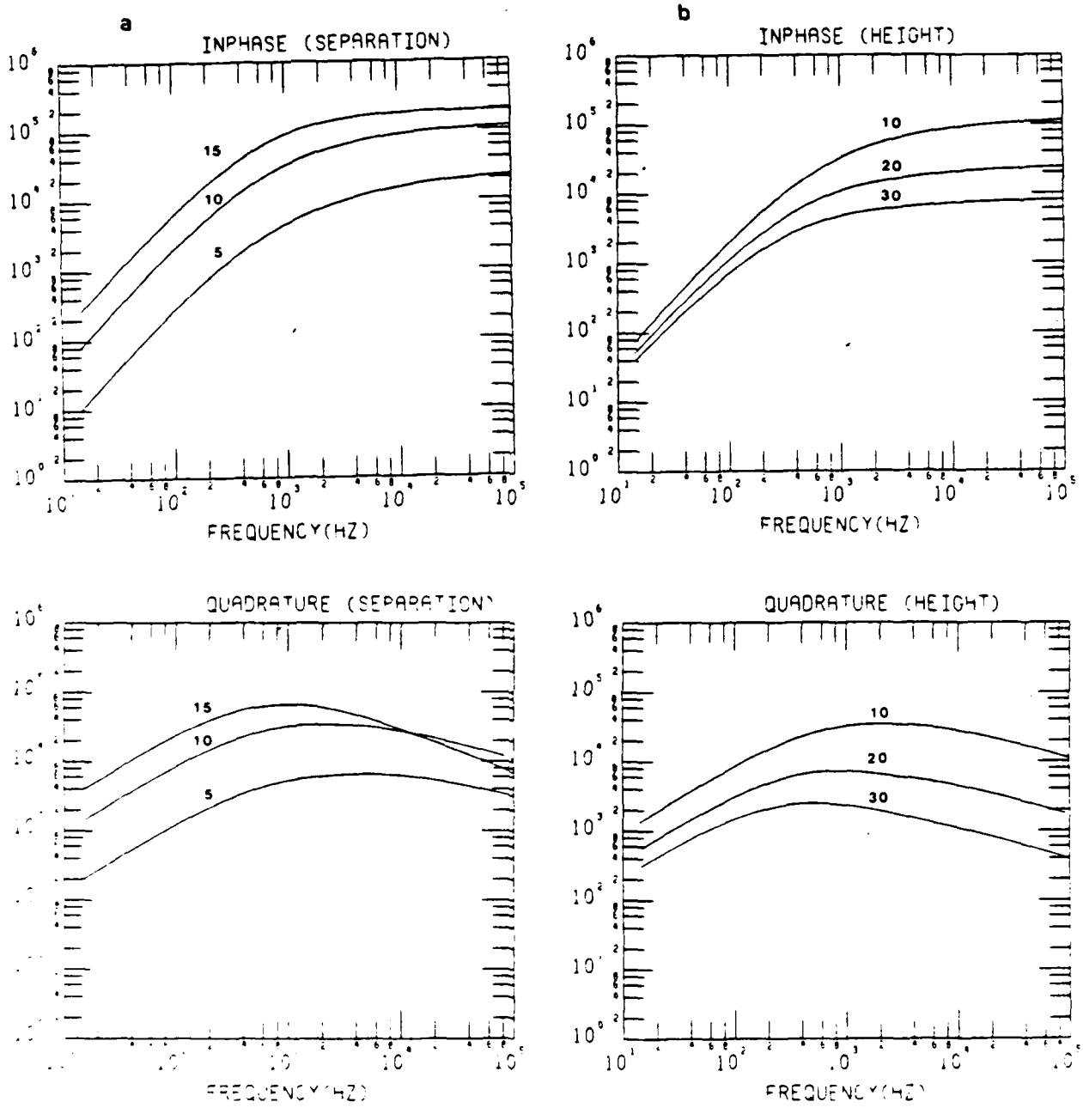

Figure 5 Effects of changes in height and coil separation for the model shown on Figure 3 (σ_1 = 2 mho/m, σ_2 = 0.2 mho/m, d = 12 m, r = h = 12 m), while keeping the other parameters the same.
a. Effect of changes in separation (5, 10, 15 m)
b. Effect of changes in heigth (10, 20, 30 m)

CORRECTIONS FOR MISPOSITION OF DIPOLES

In the airborne measurement, there are three possible errors in positioning the transmitting and receiving loops; i) deviation of the bird from a horizontal plane, ii) change of the distance between the two loops, and iii) error in the altimeter height of the bird. This section will be devoted to investigating the effect of each of these errors in the horizontal coplanar and vertical coaxial systems. We will also discuss methods of correcting for these errors.

Effect of The Bird Inclination

Let us consider a rigid bar along which horizontal coplanar coils are mounted. The bar is inclined at an angle θ with respect to the surface as shown in Figure 6.

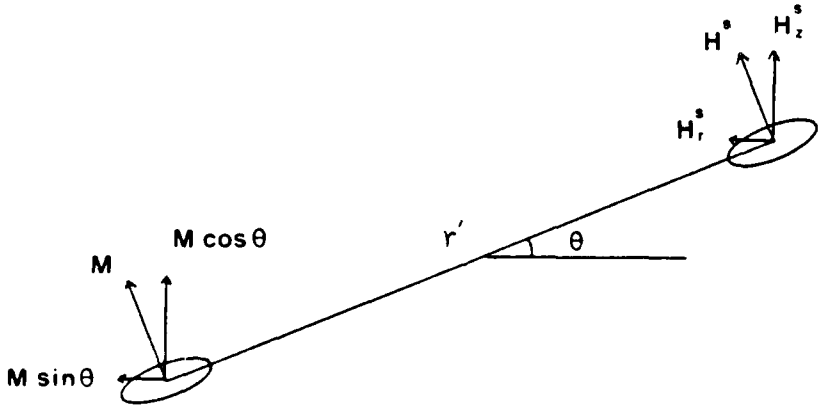

Figure 6 Horizontal coplanar coils tilted by an angle θ.

As long as the tilt angle for transmitting and receiving loops remains the same, the primary field does not change. Verma (1973) have considered the effect of ground slope in combination with transmitter coil misorientation, neglecting the effect on the primary field. The secondary fields are not affected by the heights of trasmitting and receiving loops individually, as long as the center of two receivers are kept the same, i.e., $(h+z)/2$ = const. However, in this case the horizontal distance between the two receivers is changed ($r \dashrightarrow r' \cos\theta$). Therefore, the error can arise from the angular deviation θ and the change in the distance r .

The magnetic dipole moment of the transmitting loop can be decomposed by $\vec{M} = M \cos\theta\, \hat{z} + M \sin\theta\, \hat{r}$. This decomposition results in the same effect as having two transmitting dipoles: a vertical dipole having a moment of $M \cos\theta$, and a horizontal dipole having a moment of $M \sin\theta$. The magnetic field at receiving loop becomes $H^{VS} \dashrightarrow H^{VS}\cos\theta$, $H^{HS} \dashrightarrow H^{HS}\sin\theta$, where the complementary superscripts V and H are to denote vertical and horizontal source dipole origin, respectively. On the receiving loop, we measure the field as a vectorial sum of the horizontal and vertical fields ($H^S = H_z^S \cos\theta + H_r^S \sin\theta$). Therefore the expression for the secondary field measured at the tilted receiving loop becomes:

$$H^S = [\cos\theta_1 \;,\; \sin\theta_1] \begin{bmatrix} H_z^{VS} & H_r^{VS} \\ H_z^{HS} & H_r^{HS} \end{bmatrix} \begin{bmatrix} \cos\theta_2 \\ \sin\theta_2 \end{bmatrix} \qquad (15)$$

where H_z^{VS} : z component of secondary magnetic field caused by vertical source dipole,

H_z^{HS} : z component of secondary magnetic field caused by horizontal source dipole,

H_r^{VS} : r component of secondary magnetic field caused by vertical source dipole, and

H_r^{HS} : r component of secondary magnetic field caused by horizontal source dipole.

θ_1 and θ_2 denote the inclination angle of the transmitting and receiving dipoles, respectively. The first bracket on the right-hand side of equation (15) represents the effect of tilting the source dipole by an angle θ_1, while the third represents the effect of tilting the receiver dipole by an angle θ_2. The expression (15) can be verified by considering following four different settings.

i) $\theta_1 = 0°$, $\theta_2 = 0°$ 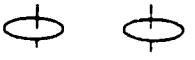 $H^S = H_z^{VS}$

ii) $\theta_1 = 0°$, $\theta_2 = 90°$ 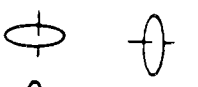 $H^S = H_r^{VS}$

iii) $\theta_1 = 90°$, $\theta_2 = 0°$  $H^S = H_z^{HS}$

iv) $\theta_1 = 90°$, $\theta_2 = 90°$ 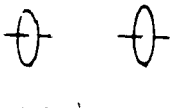 $H^S = H_r^{HS}$

From equations (2) through (6) we have,

$$H_z^{HS} = - H_r^{VS} \qquad (16)$$

$$H_r^{HS} = H_z^{VS} - \frac{M}{4\pi} \frac{1}{r} t_2 \qquad (17)$$

Substituting equations (16) and (17) into (15) and letting $\theta_1 = \theta_2 = \theta$, we obtain the expression for the secondary mag-

netic field

$$H^s = Hz^{vs} - \left(\frac{M}{4\pi} - t_z\right) \sin^2\theta \qquad (18)$$

Corresponding mutual coupling ratio Z_1'' is obtained by dividing equation (18) by a primary field $-\frac{M}{4\pi r'^3}$,

$$Z_1'' \ (= H^s/Hz^p) = Z_1' - Z_3' \sin^2\theta \qquad (19)$$

where $$Z_1' = -r'^3 \ t_o(r'\cos\theta) \qquad (20)$$

$$Z' = -r'^3 \ t_z(r'\cos\theta) \ / \ \cos 0$$

Similarly, for the horizontal dipole (Figure 7) the secondary field measured at tilted receiver dipole becomes

$$H^s = [\cos\theta_1 \ , \ -\sin\theta_1 \ ] \begin{bmatrix} Hr^{HS} & Hz^{HS} \\ Hr^{VS} & Hz^{VS} \end{bmatrix} \begin{bmatrix} \cos\theta_2 \\ -\sin\theta_2 \end{bmatrix} \qquad (21)$$

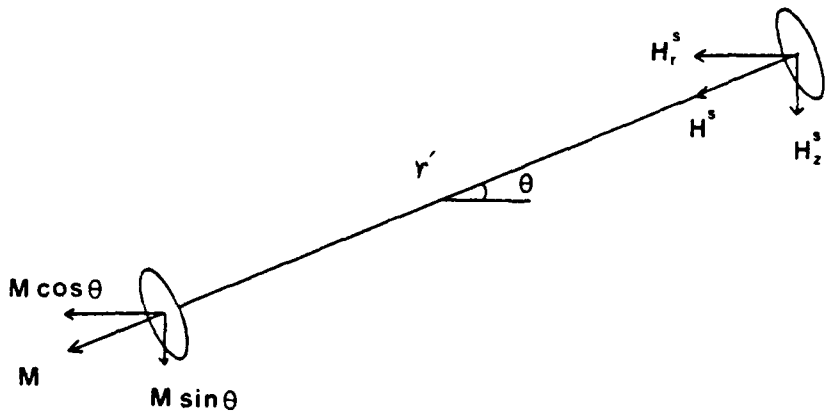

Figure 7 Vertical coaxial coils tilted by an angle θ.

and corresponding mutual impedance ratio Z_4'' is

$$Z_4'' \ (= H^s/H_r^p) = Z_4' - (1/2) \cdot Z_3' \sin^2\theta \qquad (22)$$

where $Z_4' = (1/2) \cdot (Z_3' - Z_1')$ (23)

The Z_1', Z_3' and Z_4' given by equation (20) and (23) are functions of $r'\cos\theta$, while the Z_1, Z_3 and Z_4 in equations (11) - (14) are functions of r $(= r')$.

The first terms on the right-hand side in equation (19) and (22) represent the effect of a change in the horizontal distance between two loops caused by tilting, while the second terms are the effect of tilt angle.

Table 1.a shows the real part of Z_1, Z_1', $-Z_3' \sin^2\theta$, and Z_1'' of tilted horizontal coplanar system for $\theta = 5^\circ$. The response function is the mutual impedance ratio in ppm, for a two-layer model where $r = 10$ m, $z = h = 10$ m, $\sigma_1 = 2$ mho/m, $d = 12$ m, and $\sigma_2 = 0.2$ mho/m (the same as shown in Figure 3). In the table, the second column (Z_1) represents the response of a horizontal coplanar loop at corresponding frequencies (given in the first column) for a horizontal bird. The third column (Z_1') shows the response with changed distance ($r' = r\cos\theta$). The fourth column ($-Z_3'\sin^2\theta$) shows the effect of tilt angle ($\theta = 5^\circ$), and the fifth column (Z_1'') the total expected response (sum of the third and fourth columns). The numbers in parentheses in the third and fifth columns represent the deviation from the response of a horizontal coplanar system (Z_1).

Because the tilt angle can be measured by an inclinometer, the horizontal distance ($r'\cos\theta$) can be calculated. Therefore, if we use $r'\cos\theta$ as a distance instead of r, the effect of change of distance is not problematic. In this model (σ_1 = 2 mho/m, σ_2 = 0.2 mho/m, d = 12 m, r = 10 m, $(h + Z)/2$ = 10 m), the actual change in distance caused by a 5° tilt angle is 3.8 cm (10 m - 10 m x $\cos 5^\circ$). The parenthetical numbers in the third column of Table 1.a show the effect of a 3.8 cm change in distance.

The second column in Table 1.b lists the resultant field, Z_1'', due to the tilt. This term is considered to be measured data. The third column in the table shows the effect of tilt angle for a half-space (infinite water depth). Comparison of this cclumn with the fourth column of Table 1.a, which is the effect of a tilt angle over 12 m deep sea water, shows that except for small deviations at intermediate frequency ranges (100 - 1000 Hz), the difference in amplitude is trivial. The contribution of water depth to a tilt angle effect is small. Therefore, the correction for the effect of tilt angle can be made by subtracting the theoretically calculated effect over a half-space. The last column in Table 1.b was obtained by subtracting the third column from the second column. The numbers in the parenthesis represent the deviation of this column from the Z_1' response in the third column of Table 1.a. If we use a rough estimate of depth in calculating ($-Z_3'\sin^2\theta$), we will have more accurate Z_1' response and

decrease the deviation. Since the tilt angle θ can be measured, we will use this Z_1' ($r'\cos\theta$) as a repsonse function for the inversion. If there are other factors affecting the change of separation of two loops other than the tilt angle (e.g., thermal expansion of the solid bar etc.), those also must be considered in calculating Z_1' response.

Imaginary component of horizontal coplanar system, and real and imaginary component of vertical coaxial system also show similar relations (Son, 1985). If the tilt angle θ is small, both the effect of tilt angle ($-Z_3'\sin^2\theta$) and the change in distance $r'\cos\theta$ become small. Depending on the amount of tilt angle (measued by an inclinometer), it is necessary to determine whether the correction must be made or can be neglected. The tolerable range of θ is highly dependent upon the conductivity of the water.

Table 1.a Effect of 5° tilt angle, real component of horizontal coplanar system, in ppm.

f(Hz)	Z_1	Z_1'	$-Z_3'\sin^2\theta$	Z_1''
1	1	1 (0)	0	1 (0)
10	41	41 (0)	-0	41 (0)
100	1978	1979 (1)	-8	1971 (-7)
1000	32132	32172 (40)	-132	32039 (-93)
10000	86829	87105 (276)	-412	86693 (-136)
100000	113120	113610 (490)	-590	113020 (-100)

Z_1 : no tilting ($r = r'$)
Z_1' : change in separation ($r = r'\cos\theta$); values in parenthesis denote deviation from Z_1 due to change in separation
$-Z_3'\sin^2\theta$: error due to tilting ($\theta = 5°$)
Z_1'' : resultant field due to the tilt; values in parenthesis denote total deviation, i.e., $Z_1 - Z_1''$

Table 1.b Correction for the effect of 5° tilt angle, real component of horizontal coplanar system, in ppm.

f(Hz)	Z_1''	$(-Z_3'\sin^2\theta)_{1/2}$	$Z_1'' + (Z_3'\sin^2\theta)_{1/2}$
1	1	-0	1 (0)
10	41	-0	41 (0)
100	1971	-15	1986 (7)
1000	32039	-134	32173 (1)
10000	86693	-412	87105 (0)
100000	113020	-590	113610 (0)

$(-Z_3'\sin^2\theta)_{1/2}$: error due to tilting ($\theta = 5°$) over half-space
$Z_1'' + (Z_3'\sin^2\theta)_{1/2}$: correction by subtracting half-space effect from Z_1''.
Values in the parenthesis represent deviation of corrected term from Z_1'.

Effect of Error in Altitude

In this section we will look at the effect of error in altitude of the bird and discuss how to correct for the error. Table 2.a shows the effect of a 1 % altitude error (10 cm) in positioning of height for the same model shown on Figure 3. The second column in the table shows the real component of the difference between Z_1 (r = 10 m) and Z_1' (r = 9.9 m). This table shows that a 1 % error in positioning height is more problematic than a 5° bird inclination.

Referring back to Figure 4.a, we note that at high frequencies the response converges asymtotically regardless of the depth of water. Table 2.b shows how the response function converges as a function of depth and frequency. The response becomes identical up to 1 ppm for water depth beyond 20 m at 10 kHz, 12 m at 25 kHz, and 8 m at 50 kHz. This saturation in the high-frequency response will occur at a shallow depth as either σ_1 or h increases. A similar phenomenon occurs in the response attributable to the sediment conductivity. This fact renders us to use the high frequency data to invert the height of the bird together with the water conductivity. For example, the real and imaginary components of Z_1 and Z_4 at frequencies 25 and 50 kHz (8 data) can be used to determine the height of the bird and conductivity of sea water, provided that the sea water is deeper than 12 m. Table 3.a illustrates the data contaminated by a 0.5 % random error, and that without error. The

data with 0.5 % error were subjected to the nonlinear least-squares (NLS) inversion to determine the height of the bird and sea water conductivity. the theoretically fitted values are listed in the last two columns of the Table. The inverted result are shown in Table 3.b. For initial values of h = 8 m, σ_1 = 1.6 mho/m, the inversion routine finds almost the true answer h = 10 m, σ_1 = 2 mho/m. In actual measurements, the particular frequency must be determined experimentally for a given bathymetric range.

Table 2.a Effect of a 1 % altitude error (10 cm) at an altitude of 10 m. Deviations from correct response are listed in ppm.
(h = z = r = 10 m, σ_1 = 2 mho/m, σ_2 = 0.2 mho/m, d = 12 m).

f (Hz)	Re(Z_1)	Im(Z_1)	Re(Z_4)	Im(Z_4)
1	0	-1	0	0
10	0	-11	0	+2
100	-13	-102	3	20
1000	-406	-548	-97	87
10000	-1490	-536	196	-9
100000	-1960	-183	99	-54

Table 2.b Responses at high frequency, in ppm.
The underlines indicate depth at which the saturation occurs for each frequency.
(h = z = r = 10 m, σ_1 = 2 mho/m, σ_2 = 0.2 mho/m, d = 12 m).

frequency	10 kHz		25 kHz		50 kHz	
	Re(Z_1)	Im(Z_1)	Re(Z_1)	Im(Z_1)	Re(Z_1)	Im(Z_1)
depth						
2 m	84351	40792	104349	23921	109883	15107
4	89755	30084	101470	19481	107955	15003
6	87953	27200	100796	20026	108073	15109
8	86902	27245	100904	20121	108070	15097
10	86762	27540	100916	20100	108070	15097
12	86823	27620	100913	20100	108070	15097
14	86854	27615	100913	20100	108070	15097
16	86857	27606	100913	20100	108070	15097
18	86855	27604	100913	20100	108070	15097
20	86854	27604	100913	20100	108070	15097
22	86854	27604	100913	20100	108070	15097

Table 3.a High-frequency data. Data with a 0.5 % random error are subjected to nonlinear least-squares inversion. Compared are data without error and theoretically fitted values.
(r = h = z = 10 m, σ_1 = 2.0 , σ_2 = 0.2 mho/m, d = 12 m).

	data with 0.5 % error		data without error		the theoretically fitted	
	25 kHz	50 kHz	25 kHz	50 kHz	25 kHz	50 kHz
Re(Z_1)	100999	108263	100913	108070	100895	108051
Im(Z_1)	20070	15118	20100	15097	20096	15095
Re(Z_4)	-17419	-17739	-17428	-17718	-17426	-17717
Im(Z_4)	-1640	-906	-1642	-904	-1643	-905

Table 3.b Nonlinear least-squares inversion results (h and σ_1).

	Initial value	Final
h	8.0 m	10.0012 m
σ_1	1.6 mho/m	1.9997 mho/m

SELECTION OF OPERATING FREQUENCIES

Once the data are corrected properly for the misposition of the bird through the methods presented in the previous sections, the next problem is to determine which data (in frequency) contain pertinent information toward a successful bathymetric interpretation for a given range of water depth. In this section, first we shall concentrate on how to determine an optimum frequency range for a given range of water depth. Next we will see an example of interpretation through the use of synthetic data.

Optimum Frequency Range

One of the first task for an airborne EM bathymetry survey is to determine the optimum frequency range for a given range of water depth. More importantly, what is the lowest frequency without which the depth determination becomes unreliable? We shall start answering this question by considering the following example.

Let us consider inversions of eight different water depths d = 10, 20, --- , 80 m, for conductivities of sea water σ_1 = 2 mho/m and bottom sediments σ_2 = 0.2 mho/m. Data are generated theoretically for six frequencies between 50 Hz and 15.8 kHz, equally spaced on a logarithmic scale (0.05, 0.16, 0.5, 1.6, 5 and 15.8 kHz), at a 10 m bird altitude with a 10 m coil separation. For a theoretically generated data set without error, we find that the nonlinear

inversion scheme yields exact answers. For a data set with errors (real data cannot be error-free), the scheme can always be made to converge (Aki and Richards, 1980).

Table 4.a shows the frequencies, skin depth, and a set of contaminated data (for d = 10 m). Table 4.b illustrates the inverted results using amplitude of coplanar system. The results indicate that, i) water conductivity is determined well within 0.25 % regardless of depth of water, ii) sediment conductivity is not determined accurately. Moreover after 50 m, it is not resolved at all (in the inversion process the sediment conductivity is allowed to vary between 0.4 - 0.001 mho/m), iii) uncertainty in the depth determination also increases along with that in the sediment conductivity for depths greater than 50 m. Error bounds in the computed depth are shown in parenthesis in Table 4.b. The lower bound is found by expanding the water depth until the rms difference between the data and the predicted response becomes more than 0.25 % assuming an insulating ocean bottom. Similarly, the upper bound is found by assuming 0.4 mho/m as the upper limit of the sediment conductivity. The width of the bounds starts to increase rapidly for water depth greater than 50 m.

As expected, the above results confirm the fact that determination of water conductivity is not problematic for a given frequency range regardless of water depth, however, determination of water depth and sediment condcutivity is highly dependent upon the lowest frequency used. The prob-

lem of determining the maximum lowest frequency, for the practical purpose, still remains.

In the linear inverse theory, determination of the unknown parameters coincides with solving a linear matrix equation:

$$y = A\ x \qquad (24)$$

where A is an nxm coefficient matrix (n is number of data, m is number of unknown parameters), x is a solution vector and y is a vector which is subjected to be fitted with the theoretical model. In the generalized inverse theory, the theoretical curve $\hat{y}$ is given by

$$\hat{y} = S\ y \qquad (25)$$

where $\hat{y}$ and y, respectively, denote the predicted and the observed and S is the information density matrix (Jackson, 1972; Glen et al., 1973). We note that $\hat{y}$ is a weighted sum of y through the rows of information density matrix. Each element in a row of S represents the relative contribution of the observed to the predicted. The diagonality of S matrixs indicates whether or not the corresponding datum significantly affects the solution.

Table 4.a Theoretically generated data (d = 10 m) at six frequencies (0.5 - 15.8 kHz). (z = h = r = 10 m, σ_1 = 2, σ_2 = 0.2 mho/m).

	Frequency (kHz)	Skin depth (m)	Data with 0.5 % error in ppm (d = 10 m)	
			Real(Z_1)	Imag.(Z_1)
1	50	50.3	542	4208
2	158	28.3	3379	11675
3	500	15.9	15610	25543
4	1,580	8.95	43502	35465
5	5,000	5.03	72682	31914
6	15,800	2.83	94424	23830

Table 4.b NLS (nonlinear least-squares) inverted results.

true depth (m)	σ_1 = 2 mho/m	σ_2 = 0.2 mho/m Inverted results		
	σ_1	σ_2	d	(bounds)
10	2.005	0.228	9.79	
20	2.004	0.179	20.10	
30	1.999	0.331	29.65	(28 - 30)
40	2.001	0.213	38.20	(34 - 42)
50	1.997	0.196	50.81	(42 - 77)
60	2.000	0.027	61.70	(45 - 80)
70	1.993	0.399	48.26	(40 - 90)
80	1.995	4.000	48.88	(40 - 90)
	(mho/m)		(m)	

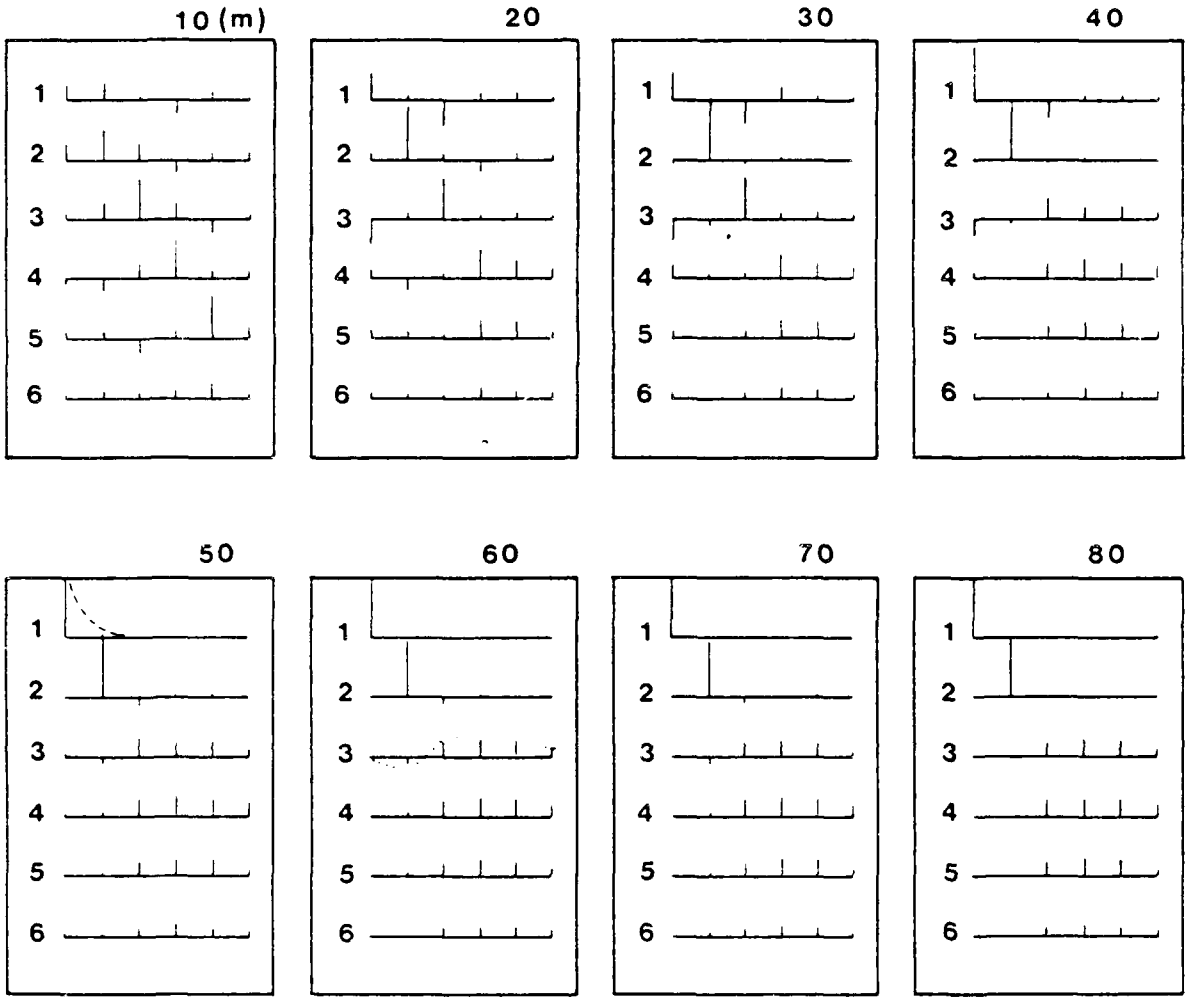

	1	2	3	4	5	6	
frequency	0.05	0.16	0.5	1.6	5	16	k Hz
skin depth	50	28	16	9	5	2.8	m

Figure 8 Information density and skin depth of six frequency data (50 - 15,800 Hz).

The information density matirices for each depth in the example are shown in Figure 8. The bottom rows of the matrix recede from a diagonal shape as the depth increases. This implies that the high-frequency data becomes less important as the depth increases. On the other hand, the contibution of lower frequencies increases as the depth increases.

Examination of the information density matrix reveals that i) the higher frequency data decrease their contribution as depth increases. There is a certain depth where the information density of some high-frequency data cease to be diagonal (shown by dotted line in the information density matrix), and that part of the data do not contribute in construction of a solution, and ii) the low frequency data increase their contribution as the depth increases; i.e., there is a certain depth where the diagonal element of a low frequency becomes unity ('saturated'). Below that depth, the contribution of the data is saturated and for a reliable result of inversion, lower frequency data are needed. This may be interpreted as follows; The coefficient matrix A in equation (24) consists of the derivatives with respect to model parameters, and the information density matrix is defined by the data space eigenvectors of A (Lanczos, 1961; Aki and Richards, 1980). Derivatives above a certain high frequency become much smaller than those of lower frequencies. Those vanishing derivatives, therefore, do not contribute in solving the equation (24). Instead, they result

in the nondiagonality of the information density matrices. Therefore, those high frequency data can be discarded safely (e.g., dotted line in the information density matrix is the starting point of nondiagonality). Meanwhile, the weight of derivatives at lower frequency increases as the depth of water increases because then high-frequency components in a column of 'A' become similar. At a certain point the weight of the low-frequency part is saturated. At that point it is necessary to have another lower frequency to achieve satisfactory resolution. In this example, the depth of saturation of the lowest frequency (dashed line in S plots) roughly coincides with the skin depth of that frequency (frequency and skin depth are shown at the bottom of each figure), and with the underlined depth of inverted result. The deviation from diagonality of S occurs when the depth of water exceeds 3 - 4 times of the skin depth. Similar analyses with different sets of frequency contents (Son, 1985) do not violate the above idea that, if the depth of investigation is deeper than the skin depth of the lowest frequency of the data, we need lower frequency data to achieve proper resolution.

Interpretation Example

Figure 9 illustrates an interpreted bathymetry profile based on a set of simulated AEMB data using six frequencies between 50 Hz and 15.8 kHz, equally spaced on a logarithmic scale (0.05, 0.16, 0.5, 1.6, 5, 15.8 kHz). Data are generated from a two-layer model in which the first layer is sea water having a conductivity of 2 mho/m underlain by a uniform bottom sediment having a conductivity of 0.2 mho/m. Simulated AEMB data are obtained for forty different water depths between 0 to 80 m at a 2 m interval at a 10 m altitude with a 10 m coil separation. A set of random numbers, whose rms amplitude is normalized to that of an infinitely long sequence, is added to contaminate the theoretical data by 0.5 %. Dotted lines in Figure 9 show the inverted depths, while the solid lines represent true depths. In all 40 inversions, the water conductivity is determined well within 0.25 % (1.9975 - 2.0046 mho/m).

The uncertainties in the water depth and sediment conductivity increase after about 40 m. The solid vertical error bars represent the uncertainty in depth. The lower bound is found by expanding the water depth until the rms difference between the data and the predicted response becomes more than 0.25 %, assuming an insulating ocean bottom. Similarly, the upper bound is found by assuming 0.4 mho/m as the conductivity of the bottom sediment. The Edge model error bounds start increasing rapidly after 50 m,

reaching infinity after 70 m.

The information distribution (diagonal elements of information density matrix) is illustrated in the inset. It shows that the contribution from low-frequency data increases as depth increases, while the high-frequency contribution increases as the water depth becomes shallow. The optimal frequency range (where the amplitude of diagonal elements of the information density matrix become bigger than 1/2) as a function of water depth is shown by a shaded area. The frequency bands within this area contribute most to the solution.

CPU times for the first (d = 2 m) and the last (d = 80 m) inversion are 0.86 sec and 3.27 sec, respectively, on an IBM 3081 mainframe computer. All least-squares inversion methods require a set of initial values which is subsequently improved through iterations (90 % of the model was used as an initial guess in this inversion). The required computer time is determined mainly by the number of iterations needed to achieve a prescribed resolution. In order to reduce the number of iterations, we have devised a "tracking" scheme in which the initial solution of the present location data will be prescribed as the final solution for the last location data point. This scheme is justified as long as the bathymetry changes gradually along the flight path. If successful, the scheme can promote significant saving in computer time for AEMB data processing.

Figure 9 Frequency-domain EM data inversion simulation, showing the bathymetry resolution up to 80 m of water depth. Simulated data are contaminated by 0.5 % random measurement errors for all cases. The sea water conductivity is resolved within 0.25 % in all cases. Resolution of the sediment conductivity is shown at the bottom. The frequency bands which contribute most to the inversion are shown as a shaded area in the inset.

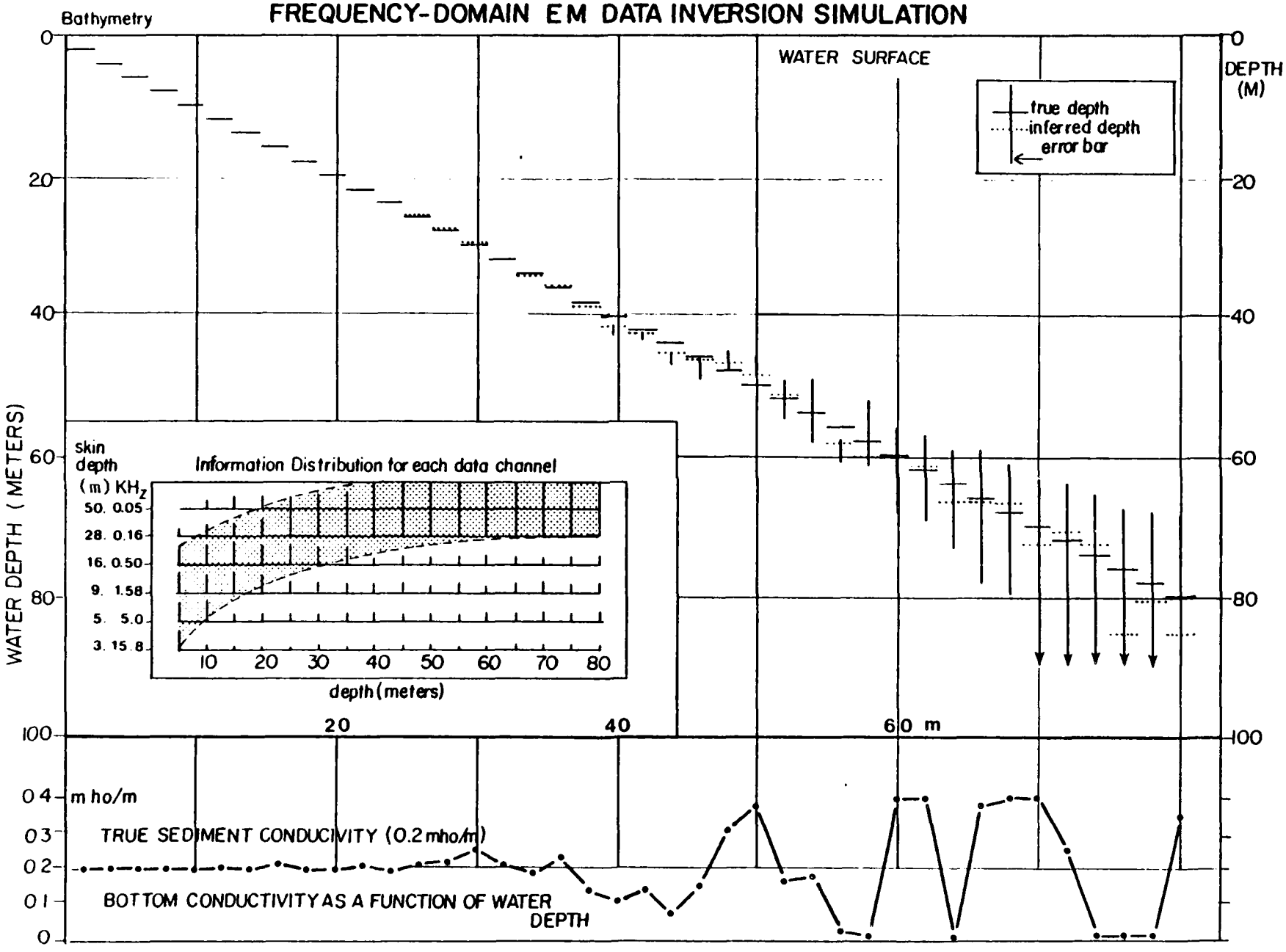
FREQUENCY-DOMAIN EM DATA INVERSION SIMULATION
Bathymetry
WATER SURFACE
DEPTH (M)
WATER DEPTH (METERS)
true depth
inferred depth
error bar
skin depth (m) KHz
Information Distribution for each data channel
50. 0.05
28. 0.16
16. 0.50
9. 1.58
5. 5.0
3. 15.8
10 20 30 40 50 60 70 80
depth (meters)
20
40
60 m
m ho/m
0.4
0.3
0.2
0.1
0
TRUE SEDIMENT CONDUCIVITY (0.2 mho/m)
BOTTOM CONDUCTIVITY AS A FUNCTION OF WATER DEPTH

Figure 9

EXPONENTIALLY DECAYING CONDUCTIVITY MODEL UNDERLAIN BY SEA WATER

Because of high conductivity of sea water, the conductivity of sediment is expected to be proportional to the porosity of bottom sediment rather than the conductivity of sediment material. Then the conductivity in the sediment layer will be decaying with depth, rather continuously than abruptly like in the layered earth model.

The continuously changing conductivity models appear in a few literatures. Mallick and Roy (1971) has derived a formula for the response of vertical magnetic dipole over transitional earth where the linear transition zone exists between the overburden and the lower half-space. Fuller and Wait (1972) has derived an expression for the high-frequency electromagnetic coupling between small coplanar loops over an inhomogeneous ground, where the conductivity of transition zone under resistive overburden increases exponentially toward the larger values of σ_2 deep within the earth. In this paper, we present a theoretical electromagnetic dipole response over exponentially decaying conductive material underlain by sea water, with the aim of investigating the conductivity of bottom sediment of sea water.

The conductivity model is shown in Figure 10.a. The σ_1 and d represent the conductivity and thickness of the sea water, respectively. The conductivity σ_2 of the bottom sediment is given by

$$\sigma_2 = \sigma_1 e^{q(z+d)}, \quad z < -d \qquad (26)$$

where q represents the decaying factor, and z represents the depth. In this model, since z is less than -d, z+d becomes negative. Therefore, if q is big, σ_2 decays fast, if q is small, σ_2 decays slowly. The conductivity of bottom layer is equal to that of sea water at the interface. At 1/q m below the interface, it becomes 1/e of the conductivity of sea water. Eventually, it becomes zero deep in the earth.

The kernel function $R(\lambda)$ in expression (10) can be replaced by (27) for the exponentially decaying conductivity model.

$$R(\lambda) = \left(\frac{n_0 - n_1}{n_0 + n_1} + \alpha \right) / \left(1 + \frac{n_0 - n_1}{n_0 + n_1} \alpha \right) \qquad (27)$$

where $\alpha = \frac{\rho n_1 - \rho'}{\rho n_1 + \rho'} e^{-z n_1 d}$ (see Appendix).

When d is set to infinity in equation (27), α becomes zero and $R(\lambda) = \frac{n_0 - n_1}{n_0 + n_1}$, which is the case of homogeneous half-space. As q approaches infinity, the conductivity of sediment decays rapidly and the model becomes the case of two-layered earth where the sea water layer is overlain by insulating bottom layer. In this case, α approaches $\frac{n_1 - \lambda}{n_1 + \lambda} e$ and equation (27) becomes identical with equation (10).

Figure 10.b shows responses of the exponentially decaying conductivity model with varying q values. In Figure 10.c, compared are the responses of two layer model with varying bottom layer conductivities. The responses are cal-

culated at 42.67 m (140 feet) altitude with 8 m coil separation. Inphase component increases as σ_z increases or q decreases. The rate of increase in exponentially decaying conductivity model is smaller than that in two layer model, especially at lower frequencies, indicating the conductivity of the former model is smaller than that of the latter at below a certain depth. The peak values of quadrature components appear at lower frequencies and becomes smaller as σ_z increases. The same phenomenon happens as q decreases, indicating that eddy current is spread in a wide range. The decay rate of peak amplitude in this case is smaller than in two layer model.

Figure 11 compares the responses of four different models. Model 1 in Figure 11.a is a two layer model where the conductivity and the depth of sea water are 4 mho/m and 4 m, respectively, and the conductivity of bottom layer is 0.01 mho/m. Model 2 is that of half-space with conductivity of 4 mho/m. Model 3 is an exponentially decaying conductivity model with q = 1, underlain by 4 m thick sea water. In model 4, the exponentially decaying part of model 3 is devided into fifty horizontal layers each having constant thickness of 10 cm. The responses are plotted in Figure 11.b (the response of model 4 is represented by '+'). The responses of model 3 and model 4 are in agreement.

Figure 10 The exponentially decaying conductivity model.
a. The exontially decaying conductivity model underlain by 4 m thick sea water. The σ_1 and σ_2 represent conductivity of sea water and sediment, respectively, and d represents the depth of water layer.
b. Response curves for the exponentially decaying conductivity model with different q values (100, 2, 1, 1/2, 1/4).
c. Response curves for two layer model with different 0 (2, 1, 0.5, 0.2, 0.001). The responses are calculated at 140 feet (42.67 m) with 8 m dipole separation.

Figure 11 Comparison of responses of four different models.
a. Geometry of four different models. Model 1 is a two layer model where the conductivity and the depth of sea water are 4 mho/m and 4 m, respectively, and the conductivity of bottom layer is 0.01 mho/m. Model 2 is that of half-space with conductivity of 4 mho/m. Model 3 is an exponentially decaying condcutivity model with q = 1, underlain by 4 m thick sea water. In model 4, the exponentially decaying part of model 3 is devided into fifty horizontal layers each having constant thickness of 10 cm.
b. The responses of four different models. The numbers on the curve coincide with those of models. The response of model 4 is plotted by '+'.

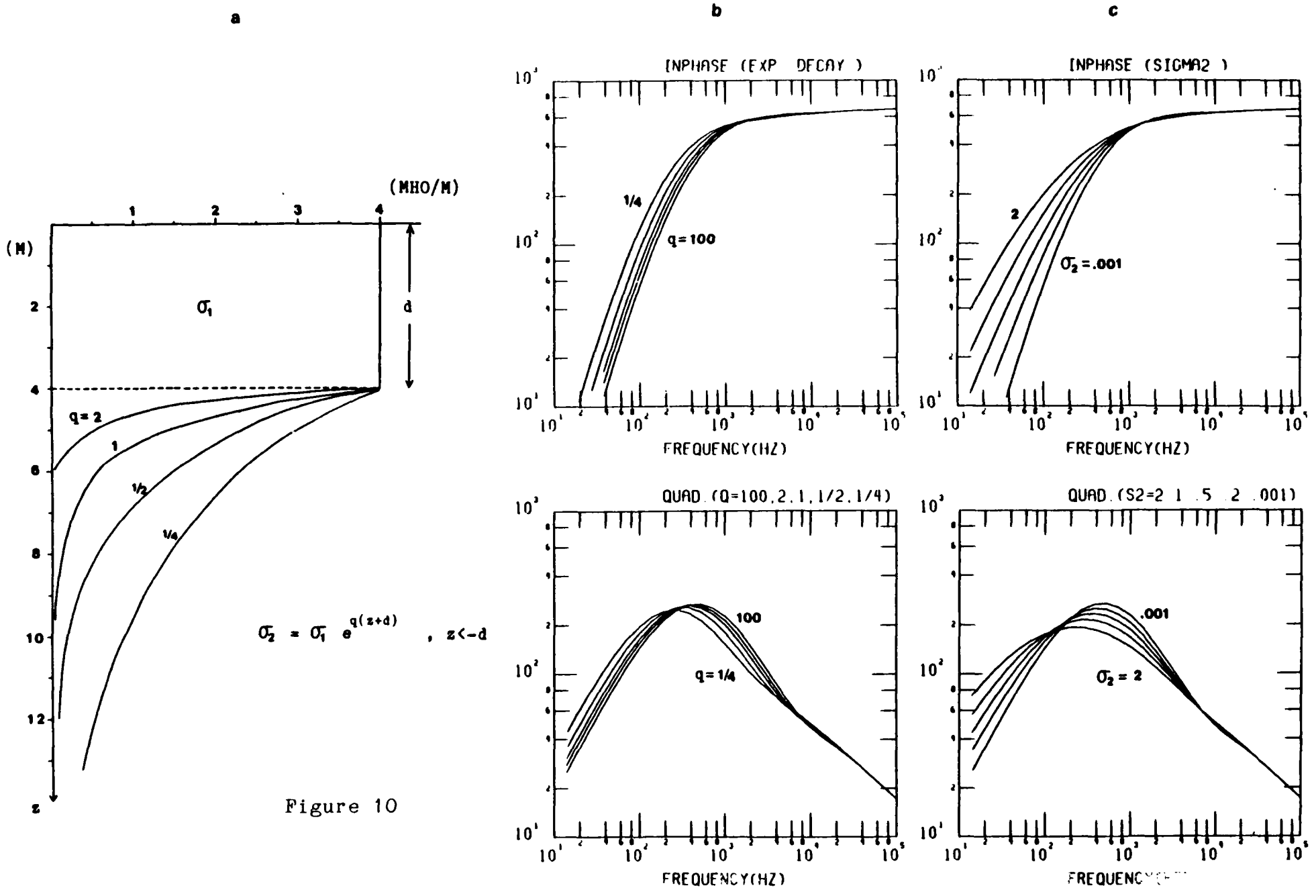
a
(MHO/M)
1
2
3
4
(M)
2
4
6
8
10
12
z
σ_1
d
q= 2
1
1/2
1/4
$\sigma_2 = \sigma_1 e^{q(z+d)}$, z<-d
b
INPHASE (EXP DECAY)
1/4
q=100
FREQUENCY(HZ)
c
INPHASE (SIGMA2)
2
σ_2=.001
FREQUENCY(HZ)
QUAD.(Q=100,2,1,1/2,1/4)
100
q=1/4
FREQUENCY(HZ)
QUAD.(S2=2 1 .5 2 .001)
.001
σ_2 = 2

Figure 10

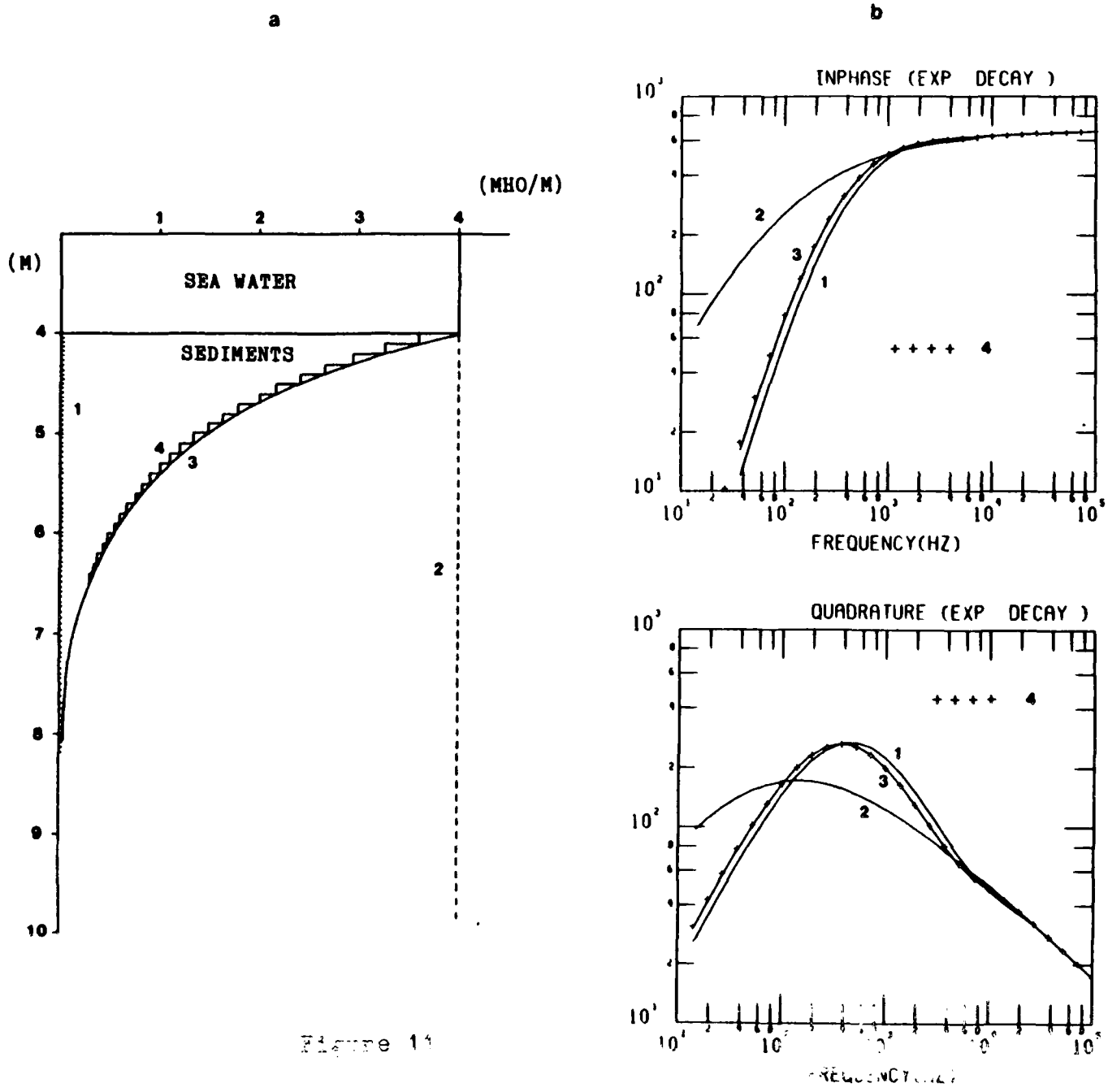
a
(MHO/M)
1
2
3
4
(M)
SEA WATER
SEDIMENTS
4
5
6
7
8
9
10
1
4
3
2
b
INPHASE (EXP DECAY)
10^3
10^2
10^1
2
3
1
+ + + + 4
10^1
10^2
10^3
10^4
10^5
FREQUENCY(HZ)
QUADRATURE (EXP DECAY)
10^3
+ + + + 4
1
3
2
10^2
10^1
10^4
10^5

Figure 11

CONCLUDING REMARKS

In the Airborne Electromagnetic Bathymetry problem, the major challenge is the skin effect of highly conductive sea water. Since most of the response is due to uppermost sea water, errors in sensor altitude and inclination can cause as much effect as bottom geometry. To increase water depth sensitivity, we are forced to lower the frequency band, which also suffers from severe practical limitations. Despite all these difficulties, the AEMB concept carries a few advantageous aspects including a) a simple geometry which may be approximated as one layer over a homogeneous half-space, b) no surface topography, c) a more or less uniform sea water conductivity within a zone below the instruments (due to rapid mixing of shelf water caused by wave action), and d) possible application of bathymetric tracking during the inversion procedure owing to gentle and gradual changes in bathymetry. These simple geometrical aspects provide us with many practical advantages needed in survey design and data interpretation.

The results in this study include i) that uncertainties in sensor altitude can be resolved through an inversion process, using high-frequency data where the effect of bottom sediments is excluded, and assuming two unknowns (altitude and sea water conductivity), ii) inclination of the coil axis with respect to the sea surface can be resolved by installing an inclinometer on the sensor platform and cor-

recting for this effect during the inversion process, iii) the optimum frequency range for operational and interpretational purposes can be determined before actual measurements, via information density matrix analysis. For the data measured at 10 m altitude with 10 m separation, it appears that, for a reliable result, at least a low frequency whose skin depth is close to the depth of investigation need be included, and that high frequencies whose skin depths are less than 1/4 - 1/3 of the depth of investigation are not important in determining the bottom geometry. Interpretation and survey design may vary depending with each situation (percentage of error included in the data, height and separation of the bird, etc.). However, the methods presented in this study could be applied in any case. Vertical heterogeneity of sea water or bottom sediment conductivity, and deviation from a horizontally layered model were not considered in the analysis.

In order to account for the effect of conductivity variation in sediment, a theoretical electromagnetic response over exponentially decaying conductivity material underlain by sea water has been derived. Comparison of the response with that of a similar multi-layered model shows agreement. Since the decaying pattern of sediment conductivity is related with the compactness of the bottom sediment, it may provide valuable information toward ocean engineering. Application of the theory presented in this paper, to real data, will be published in next paper.

APPENDIX

Derivation of a kernel function for exponentially decaying conductivity model

In this appendix, we will derive a response function (mutual coupling ratio) of the horizontal coplanar system over a exponentially decaying conductivity model underlain by highly conductive sea water (Figure 10.a). The electrical permittivity (ϵ) and the magnetic permeability (μ) of the earth will be assumed the same as those of the air. The displacement current in the earth is neglected.

In time-harmonic electromagnetic field, the magnetic vector potential A satisfies the Helmholtz equation (Patra and Mallick, 1980):

$$\nabla^2 \vec{A} + \gamma^2 \vec{A} = 0 \qquad (A-1)$$

where $\gamma^2 = iw\mu\sigma$, $i = \sqrt{-1}$, w angular frequency and σ is conductivity of the material. For the horizontal dipole over vertical stratification, the vector wave equation (A-1) reduces to a scalar wave equation in cylinderical coordinate (r, θ, φ):

$$\frac{\partial^2 A_z}{\partial r^2} + \frac{1}{r}\frac{\partial A_z}{\partial r} + \frac{\partial^2 A_z}{\partial z^2} + \gamma^2 A_z = 0 \qquad (A-2)$$

where A_z is z component of the vector potential $\vec{A}$. Separating the variables: A(=Az) = R(r) Z(z), and substituting this expression into equation (A-2), we obtain two

ordinary differential equations:

$$\frac{d^2R}{dr^2} + \frac{1}{r}\frac{dR}{dr} + \lambda^2 R = 0 \qquad (A-3)$$

$$\frac{d^2Z}{dz^2} - \{ \gamma^2(z) + \lambda^2 \} Z = 0 \qquad (A-4)$$

where λ is a separation constant. A non-divergent solution of equation (A-3) is $J_o(\lambda r)$: Bessel's function of order zero. The solution for equation (A-4) depends upon $\gamma^2(z)$. For a layered earth model, a general solution of the vector potential above the surface of the earth is written as a Hankel transform integral:

$$A = C \left\{ \frac{1}{r} + \int_o^\infty R(\lambda)\, e^{-\lambda(h+z)}\, J_o(\lambda r)\, d\lambda \right\} \qquad (A-5)$$

where C is a constant, r is the distance between two loops, h and z are, respectively, the heights of transmitting and receiving loops, and $R(\lambda)$ is a kernel function including geological parameters. The kernel function for a two layered earth is given by equation (10).

When we consider the exponentially decaying conductivity model underlain by highly conductive sea water (Figure 10.a), the radiation constants in each region can be written as,

$$\text{(sea water)}: \quad \gamma_1^2 = iw\mu\sigma_1$$

$$\text{(sediment)}: \quad \gamma_2^2 = iw\mu\sigma(z) = iw\mu\sigma_1 e^{q(z+d)} = \gamma_1^2 e^{q(z+d)}$$

Then, the equation (A-4) in the sediment layer becomes,

$$\frac{d^2 Z}{dz^2} - \{ \gamma_1^2 e^{q(z+d)} + \lambda^2 \} Z = 0 \qquad (A-6)$$

Making a substitution of the form

$$x(z) = \gamma_1^2 e^{q(z+d)}$$

we can derive

$$\frac{dx}{dz} = q\,x$$

and $$\frac{d^2 Z}{dz^2} = \frac{d^2 Z}{dx^2} (q\,x)^2 + \frac{dZ}{dx} q^2 x$$

With these expressions, equation (A-6) becomes

$$q^2 x^2 \frac{d^2 Z}{dx^2} + q^2 x \frac{dZ}{dx} - (x + \lambda^2) Z = 0$$

In this equation if q is not equal to zero (If q = 0, it becomes the case of two layer model.), we obtain a linear homogeneous second-order differential equation with a regular singular point (Arfken, 1971) at x = 0:

$$\frac{d^2 Z}{dx^2} + \frac{1}{x} \frac{dZ}{dx} - \frac{x + \lambda^2}{q^2 x^2} Z = 0 \qquad (A-7)$$

A solution of this equation can be secured by Frobenius' method assuming the solution of the form,

$$Z(x) = \sum_{j=0}^{\infty} a_j x^{k+j} \qquad (a_0 \neq 0) \qquad (A-8)$$

where k is a constant. Substituting the expression (A-8) into equation (A-7), we derive a non-diverging solution

$$Z(x) = a_0 \sum_{j=0}^{\infty} \frac{x^{(\frac{\lambda}{q}+j)}}{(jq)!\,(jq+2\lambda)!} \qquad (A-9)$$

where $\gamma_1^2 < x = \gamma_1^2 e^{q(z+d)} < 0$, $q \neq 0$ and $(jq + 2\lambda)! = 1$, for $j = 0$.

Let us write

$$P(z) = \sum_{j=0}^{\infty} \frac{\left\{ \gamma_1^2 \, e^{q(z+d)} \right\}^{\frac{\lambda}{q}+j}}{(jq)! \; (jq + 2\lambda)!}$$

Then, $Z(z) = a_0 \, P(z)$

The corresponding solutions in different layers are:

$$\text{Air} : \quad A^1 = C \left\{ \frac{1}{r} + \int_0^{\infty} A(\lambda) e^{-n_0 z} \, J_0(\lambda r) \, d\lambda \right\}$$

$$\text{Sea-Water} : \quad A^2 = \int_0^{\infty} \{ B_1(\lambda) \, e^{n_1 z} + B_2(\lambda) \, e^{n_1 z} \} \, J_0(\lambda r) \, d$$

$$\text{Lower Half-Space} : \quad A^3 = \int_0^{\infty} D(\lambda) \, P(z) \, J_0(\lambda r) \, d\lambda$$

where $n_i = \sqrt{\lambda^2 + \gamma_i^2}$, $i = 0, 1, 2$. The $A(\lambda)$, $B_1(\lambda)$, $B_2(\lambda)$ and $D(\lambda)$ are coefficents which will be determined from boundary conditions.

Applying the boundary conditions (the tangential components of elctric and magnetic field vectors must be continuous accross the surface) at $z = 0$ and $-d$, we can derive

$$A(\lambda) = \left(\frac{n_0 - n_1}{n_0 + n_1} + \alpha \right) / \left(1 + \alpha \frac{n_0 - n_1}{n_0 + n_1} \right), \qquad \text{(A-10)}$$

$$\alpha = \frac{P n_1 - P'}{P n_1 + P'} \, e^{-2 n_1 d},$$

$$P = P(-d) = \sum_{j=0}^{\infty} \frac{\gamma_1^{2(\frac{\lambda}{q}+j)}}{(jq)! \; (jq + 2\lambda)!}$$

$$\text{and} \quad P' = \left. \frac{\partial P}{\partial z} \right|_{z=-d} = \sum_{j=0}^{\infty} \frac{(\lambda + jq) \, \gamma_1^{2(\frac{\lambda}{q}+j)}}{(jq)! \; (jq + 2\lambda)!}$$

This is the kernel function for exponentionally decaying conductivity model underlain by sea water.

Convergence Consideration

Before we consider numerical convergence, let us consider two limiting case of the kernel function. When d is set to infinity in equation (A-10), the model becomes a half-space having sea water conductivity. In this case α becomes zero and $R(\lambda) = \frac{n_0 - n_1}{n_0 + n_1}$, which is identical with the kernel function of a half-space. This is a confirmation of the result in (A-10). When q becomes infinity, the model approaches a two-layered one having zero conductivity in the second layer. In this case, P and P' in (A-10) become, $\lim_{q \to \infty} P = 1$ and $\lim_{q \to \infty} P' = \lambda$. Then,

$$\lim_{q \to \infty} \alpha = \frac{n_1 - \lambda}{n_1 + \lambda} e^{-2 n_1 d}$$

This being substituted into (A-10), the kernel function becomes identical with expression (10) for a two layer model having zero second layer conductivity. This is another confirmation of the result.

Convergence of P and P' in (A-10) is dependent upon the value of q. If q is big they converge fast. If q is small they converge slowly. The decaying factor q determines the decay rate of sediment conductivity. For example, if q = 1 (1/m), σ_2 becomes 1/e of σ_1 at 1 m below the water-sediment interface. If q = 0.1, σ_2 becomes 1/e of σ_1 at 10 m below the interface. At q = ∞ which is the case of two layer model having infinitively resistive second layer, the first terms in the series are dominant. As q decreases (σ_2 decays

slowly), the higer terms are added and convergence becomes slower.

Referring back to the derivation of equation (A-7), the result in (A-10) is valid only for q = 0. Moreover as q approaches zero, numerical convergence may confront serious problem (limitation of the result). However, the case of extremely small q (less than 0.01) is rare in reality. If we are considering q bigger than 0.1 like in the bathymetry problem, the convergence is not problematic.

ACKNOWLEDGEMENT

We thank Dr. M.G. Bevis at North Carolina State University for his valuable comments in geophysical inverse theory. This research has been supported by Army Research Office, Research Triangle Park, North Carolina, through Contract DAAG29-83-K-0152.

List of References

Aki, K., and Richards, P.G., 1980, Quantitative seismology, W.H.Freeman and Company, San Francisco.

Arfken, G., 1971, Mathematical methods for physicists, Academic Press Inc., New York.

Becker, A., Morrison, H.F., Zollinger, R., and Lazenby, P.G., 1984, Airborne Electromagnetic Bathymetry, 54th Annual International SEG Meeting, Extended Abstracts.

Frischknect, F.C., 1967, Fields about an oscillating magnetic dipole over a two-layer earth, and application to ground and airborne electromagnetic Surveys: Quarterly of the Colorado School of Mines, v. 62, no. 1.

Fuller, J.A., and Wait, J.R., 1972, High-frequency electromagnetic coupling between small coplanar loops over an inhomogeneous ground: Geophysics, v. 37, no. 6, p. 997-1004.

Grant, F.S., and West, G.F., 1965, Interpretation Theory in Applied Geophysics, Mcgraw-Hill book Company, New York.

Glen, W.E., Ryu, J., Ward, S.H., Peeples, W.J., and Phillips, R.J., 1973, The inversion of vertical magnetic dipole sounding data: Geophysics, v. 38, no. 6, p. 1109-1129.

Inman, J.R., Ryu, J., and Ward, S.H., 1973, Resistivity inversion: Geophysics, v. 38, no. 6, p. 1088-1108.

Jackson, D.D., 1972, Interpretation of inaccurate, insufficient and inconsistent data: Geophys.J.R.Astron.Soc., v. 28, p. 97-109.

Kaufman, A.A., and Keller, G.V., 1983, Frequency and Transient Soundings, Elsevier Pub., Amsterdam.

Lanczos, C., 1961, Linear Differential Operators, D. van

Nostrand Co. LTD., London.

Marquardt, D.W., 1963, An algorithm for least-squares estimation of nonlinear parameters: J.Soc.Indust.Appl.Math., v. 11, p. 431-441.

-------, 1970, Generalized inverse, ridge regression, biased linear estimation, and nonlinear estimation: Technometrics, v. 12, p. 69-82.

Mallick, K., and Roy, A., 1971, Vertical Magnetic Dipole over Transitional Earth: Geophysical Prospecting, v. 19, p. 388-394.

Patra, H.P., and Mallick, K., 1980, Geosounding Principles 2, Elsevier Pub., Amsterdam.

Son, K.H., 1985, Interpretation of electromagnetic dipole-dipole frequency sounding data over a vertically stratified earth, A Ph.D Thesis, North Carolina State University, North Carolina.

Verma, R.K., 1973, Topographic effects on electromagnetic depth sounding systems: Geophysical prospecting, v. 21, p. 1-25.

Wait, J.R., 1951, The magnetic dipole over the horizontally stratified earth: Can.J.Phys., v. 29, p. 577-592.

Ward, S.H., 1967, Electromagnetic theory for geophysical application in Mining Geophysics: v. 2 : Tulsa, SEG.

Wiggins, R.A., 1972, The general linear inverse problem: implication of surface waves and free oscillations for Earth structure: Rev.Geophys.Space Phys., v. 10, p. 251-285.

END

DTIC

7-86